Astrodynamics Vol. 3, No. 1, 61–77, 2019 https://doi.org/10.1007/s42064-018-0036-7

Nonlinear semi-analytical uncertainty propagation of trajectory under impulsive maneuvers

Zhen Yang, Ya-Zhong Luo (✉), and Jin Zhang

College of Aerospace Science and Engineering, National University of Defense Technology, Changsha 410073, China

ABSTRACT

The usage of state transition tensors (STTs) was proved as an effective method for orbital uncertainty propagation. However, orbital maneuvers and their uncertainties are not considered in current STT-based methods. Uncertainty propagation of spacecraft trajectory with maneuvers plays an important role in spaceflight missions, e.g., the rendezvous phasing mission. Under the effects of impulsive maneuvers, the nominal trajectory of a spacecraft will be divided into several segments. If the uncertainty is piecewise propagated using the STTs one after another, large approximation errors will be introduced. To overcome this challenge, a set of modified STTs is derived, which connects the segmented trajectories together and allows for directly propagating uncertainty from the initial time to the final time. These modified STTs are then applied to analytically propagate the statistical moments of navigation and impulsive maneuver uncertainties. The probability density function is obtained by combining STTs with the Gaussian mixture model. The proposed uncertainty propagator is shown to be efficient and affords good agreement with Monte Carlo simulations. It also has no dimensionality problem for high-dimensional uncertainty propagation.

KEYWORDS

uncertainty propagation
state transition tensors (STTs)
Gaussian mixture model
rendezvous phasing

Research Article

Received: 13 June 2018
Accepted: 6 October 2018

1 Introduction

With the number of tracked space objects growing sharply, the efficient and accurate propagation of their orbital uncertainties becomes an essential issue in space situational awareness (SSA). Orbital uncertainty propagation is a common requirement to many SSA functions including tracking and data association, conjunction analysis and probability of collision, sensor resource management, and anomaly detection [1]. The propagation of uncertainty in astrodynamics is usually addressed by linear models [2, 3] or nonlinear Monte Carlo (MC) simulations [4, 5]. The linear methods are computationally efficient, but their accuracy declines for highly nonlinear systems or long-duration propagations. Conversely, MC simulations provide high-precision statistics, but are computationally expensive. To avoid these shortcomings, many analytical or semi-analytical techniques for nonlinear uncertainty propagation have been developed in recent years.

Junkins *et al.* [6, 7] first investigated the nonlinear, non-Gaussian characteristics of orbit uncertainty propagation in different coordinate systems. They found that the orbital-element expression has better accuracy than the Cartesian coordinate expression on uncertainty prediction. Julier and Uhlmann [8] proposed an unscented transformation method based on the idea that it may be easier to approximate the probability distribution than to approximate the nonlinear transformation for a given dynamical system. Park and Scheeres [9] proposed a semi-analytical state transition tensors (STTs) method by solving the higher-order Taylor series expansions that describe the localized nonlinear motion. This approach has been further developed by Fujimoto *et al.* [10] and Park and Scheeres [11]. Yang *et al.* [12] employed the STT-based method to determine the required navigation precision for a short rendezvous mission. With the similar concept of STTs, Hernando-Ayuso and Bombardelli [13] developed an analytical second-order solution for relative orbit

✉ luoyz@nudt.edu.cn

uncertainty propagation in nearly circular orbits, and Yang *et al.* [14] proposed an analytical second-order solution for relative orbit uncertainty propagation in J_2-perturbed elliptic orbits. The STT-based methods are efficient and accurate for uncertainty propagation. However, they require the derivation of higher-order partials of the governing differential equations, which could be very complex for high-fidelity orbital dynamics. In comparison to the STT method, the differential algebraic (DA) technique can automatically expand the flow of the dynamics up to an arbitrary order within a computerized environment, thus can avoid manually deriving the higher-order partials. The DA was first proposed by Berz [15], then was applied to propagate orbital uncertainty by Valli *et al.* [16]. The DA-based uncertainty propagator has been used to solve different problems in Refs. [17–19]. Both the STTs and the DA are intrusive methods that require a modification of either the system model or the algebra used to evaluate the quantities of interest. Similarly, Riccardi *et al.* [20] developed another intrusive method to propagate orbital uncertainty based on Tchebycheff polynomial algebra. On the contrary, Jones *et al.* [21–23] proposed a non-intrusive polynomial chaos (PC) method for orbital uncertainty propagation. The non-intrusive PC method treats the governing dynamics as a black-box and thus does not need any simplifications on the dynamics. However, it suffers from the dimensionality problem. A comparison between the intrusive and non-intrusive uncertainty propagators is given by Vetrisano and Vasile [24].

As proved by the previous studies [9–24], the initial Gaussian distribution becomes non-Gaussian after a nonlinear mapping. In order to fully describe the non-Gaussian distribution, it requires the propagation of the probability density function (PDF) governed by Fokker–Planck equation (FPE) [25], which is extremely difficult for high-dimensional systems, e.g., the 6-dimensional orbital dynamics. Alternatively, the Gaussian mixture model (GMM) method can approximate the PDF of an arbitrarily non-Gaussian distribution without solving the FPE. Therefore, several GMM methods have been developed by Horwood *et al.* [26], DeMars *et al.* [27], Vishwajeet *et al.* [28], and Vittaldev and Russell [29]. The GMM method decouples a large uncertainty propagation problem into many small problems, which is an effective methodology to represent a non-Gaussian distribution and to reduce the effects of nonlinearity in dynamics. This concept can be commonly combined with other uncertainty propagators to develop some hybrid methods, e.g., the GMM and STT method [30] and the GMM and PC method [31]. For more discussions of different uncertainty propagation methods, readers can refer to the review paper given by Luo and Yang [32].

The advantages of STT-based methods are twofold: (1) only the statistics (e.g., mean and covariance matrix) of the input uncertainty are required, thus the curse of dimensionality can be avoided as no randomized samples are needed, and (2) the propagation of statistics is just an algebraic manipulation once the STTs are integrated along the reference trajectory, which makes these methods very efficient. However, most previous STT methods did not consider the effects of orbital maneuvers. Although the orbital maneuvers were included in Yang *et al.* [12], their method was only suitable for short duration propagations, because the statistics in their method were propagated by repeatedly using STTs in each segmented trajectory, which would make the approximation errors repeatedly enlarged by the segmented STTs.

In order to include the effects of orbital maneuvers, this study develops an STT-based, semi-analytical orbital uncertainty propagation method. First, a set of modified STTs which connects two segmented trajectories is formulated using the original STTs proposed by Ref. [9], and then these modified STTs are used to propagate navigation and impulsive maneuver uncertainties from initial time to the final time. Finally, the modified STTs are combined with a GMM to propagate the PDF of a multivariate non-Gaussian distribution. This combined GMM and STT method allows for efficiently nonlinear, non-Gaussian uncertainty propagation as all the Gaussian mixtures can be mapped using the same STTs.

This manuscript is organized as follows. Section 2 provides the basic models for the related uncertainties and describes the uncertainty propagation problem. Section 3 derives the computational equation of the modified STTs, followed by the STT-based uncertainty propagator in Section 4. Numerical results and comparisons are presented in Section 5, and conclusions are finally drawn in Section 6.

2 Problem statement

2.1 Orbital dynamics

Considering the perturbations of J_2 term and atmospheric drag, the spacecraft's orbital dynamics in

the Earth's J2000 inertial coordinate system are given as follows [33]:

$$\begin{cases} \dot{x} = v_x, \quad \dot{y} = v_y, \quad \dot{z} = v_z \\ \dot{v}_x = -\dfrac{\mu x}{r^3} + \dfrac{3\mu J_2 R_{\mathrm{e}}^2}{2r^5}\left(\dfrac{5z^2}{r^2} - 1\right) x \\ \qquad -\dfrac{1}{2}\dfrac{C_{\mathrm{D}} S}{M}\rho v_{\mathrm{rel}}(v_x + \omega_{\mathrm{e}} y) + \Gamma_x \\ \dot{v}_y = -\dfrac{\mu y}{r^3} + \dfrac{3\mu J_2 R_{\mathrm{e}}^2}{2r^5}\left(\dfrac{5z^2}{r^2} - 1\right) y \\ \qquad -\dfrac{1}{2}\dfrac{C_{\mathrm{D}} S}{M}\rho v_{\mathrm{rel}}(v_y - \omega_{\mathrm{e}} x) + \Gamma_y \\ \dot{v}_z = -\dfrac{\mu z}{r^3} + \dfrac{3\mu J_2 R_{\mathrm{e}}^2}{2r^5}\left(\dfrac{5z^2}{r^2} - 3\right) z \\ \qquad -\dfrac{1}{2}\dfrac{C_{\mathrm{D}} S}{M}\rho v_{\mathrm{rel}} v_z + \Gamma_z \end{cases} \tag{1}$$

where μ, ω_{e}, R_{e}, and J_2 are the Earth's gravitational constant, rotation angular velocity, average equatorial radius, and J_2-perturbation coefficient, respectively; $\boldsymbol{x} = [\boldsymbol{r}, \boldsymbol{v}]^{\mathrm{T}}$ denotes the spacecraft's state, $\boldsymbol{r} = [x, y, z]^{\mathrm{T}}$ and $\boldsymbol{v} = [v_x, v_y, v_z]^{\mathrm{T}}$ are the position and velocity vector, respectively; $r = \|\boldsymbol{r}\|$, and $\|\cdot\|$ denotes the Euclid norm of a vector. Additionally, $v_{\mathrm{rel}} = \sqrt{(v_x + \omega_{\mathrm{e}} y)^2 + (v_y - \omega_{\mathrm{e}} x)^2 + v_z^2}$ is the spacecraft's velocity relative to the atmosphere, C_{D} is the coefficient of drag, S is the cross-sectional area of the spacecraft, M is the mass of the spacecraft, and $\boldsymbol{\Gamma} = [\Gamma_x, \Gamma_y, \Gamma_z]^{\mathrm{T}}$ is the thrust acceleration vector. If the impulsive thrust is assumed, the post-maneuver position and velocity vectors can be expressed as

$$\begin{aligned} &\boldsymbol{r}^+(t_i) = \boldsymbol{r}(t_i), \quad i = 1, 2, \cdots, m \\ &\boldsymbol{v}^+(t_i) = \boldsymbol{v}(t_i) + \Delta\boldsymbol{v}_i \end{aligned} \tag{2}$$

where the superscript "+" denotes the post-maneuver state, t_i is the ith maneuver time, and m is the number of impulses.

2.2 Uncertainty models

According to Ref. [34], the differences between the actual and nominal trajectories are mainly caused by three error sources: dynamic model errors, navigation errors, and actuation errors. *Dynamic model errors* are the differences between the normally used model parameters and the real values of the model parameters, e.g., the atmospheric density, and the gravity field parameters. *Navigation errors* are the differences between the state as perceived by the measurement system and the real state (position, velocity, attitude, and angular rate) of the spacecraft. Initial navigation errors can be amplified over time by effects of orbital dynamics and thrust maneuvers. *Actuation errors* are the differences between the proper corrections of the values to be controlled and the ones actually produced by the actuator; these errors are caused by the spacecraft's thruster and control system.

For the near-Earth orbits, the main dynamic model errors are the atmospheric parameters since the Earth's gravity field is relatively accurate. This paper mainly concerns about the formulation of a set of modified STTs and their application in uncertainty propagation under impulsive maneuvers, thus the dynamic model errors are not considered. However, the approach presented in Yang *et al.* [12] can be used to take model errors into account.

Assuming that the measured or predicted state of a spacecraft is $[\boldsymbol{r}_0, \boldsymbol{v}_0]^{\mathrm{T}}$, then its real state $[\tilde{\boldsymbol{r}}_0, \tilde{\boldsymbol{v}}_0]^{\mathrm{T}}$ with navigation uncertainty can be expressed as

$$\begin{aligned} \tilde{\boldsymbol{r}}_0 &= \boldsymbol{r}_0 + \delta\boldsymbol{r}_0 \\ \tilde{\boldsymbol{v}}_0 &= \boldsymbol{v}_0 + \delta\boldsymbol{v}_0 \end{aligned} \tag{3}$$

where $[\delta\boldsymbol{r}_0, \delta\boldsymbol{v}_0]^{\mathrm{T}}$ is a random realization of the navigation uncertainty.

Assuming that the nominal impulsive maneuvers are $\Delta\boldsymbol{v}_i = [\Delta v_{ix}, \Delta v_{iy}, \Delta v_{iz}]^{\mathrm{T}} (i = 1, 2, \cdots, m)$, then the real impulse $\Delta\tilde{\boldsymbol{v}}_i$ with maneuver uncertainty can be expressed as

$$\begin{aligned} &\Delta\tilde{\boldsymbol{v}}_i = \Delta\boldsymbol{v}_i + \delta\Delta\boldsymbol{v}_i, \quad i = 1, 2, \cdots, m \\ &\sigma(\delta\Delta\boldsymbol{v}_{ij}) = \alpha\,|\Delta\boldsymbol{v}_{ij}| + \beta, \quad j = x, y, z \end{aligned} \tag{4}$$

where $|\cdot|$ denotes the absolute value, $\delta\Delta\boldsymbol{v}_i$ is a random realization of the impulsive maneuver uncertainty, its standard deviations, $\sigma(\delta\Delta\boldsymbol{v}_{ij})$, is proportional to the magnitude of $\Delta\boldsymbol{v}_{ij}$, and α and β are the coefficients. It is noted that the three coordinates of a maneuver uncertainty can be chosen as corrected by setting the non-diagonal elements of its covariance matrix as nonzero, as shown in Eq. (31).

2.3 Uncertainty propagation with maneuvers

Figure 1 illustrates the uncertainty propagation process under impulsive maneuvers. The nominal impulsive maneuvers $\Delta\boldsymbol{v}_i (i = 1, 2, \cdots, m)$ are first preplanned using the chaser's initial navigation state $[\boldsymbol{r}_0, \boldsymbol{v}_0]^{\mathrm{T}}$ and final aimed state $[\boldsymbol{r}_{\mathrm{aim}}, \boldsymbol{v}_{\mathrm{aim}}]^{\mathrm{T}}$. The uncertainty

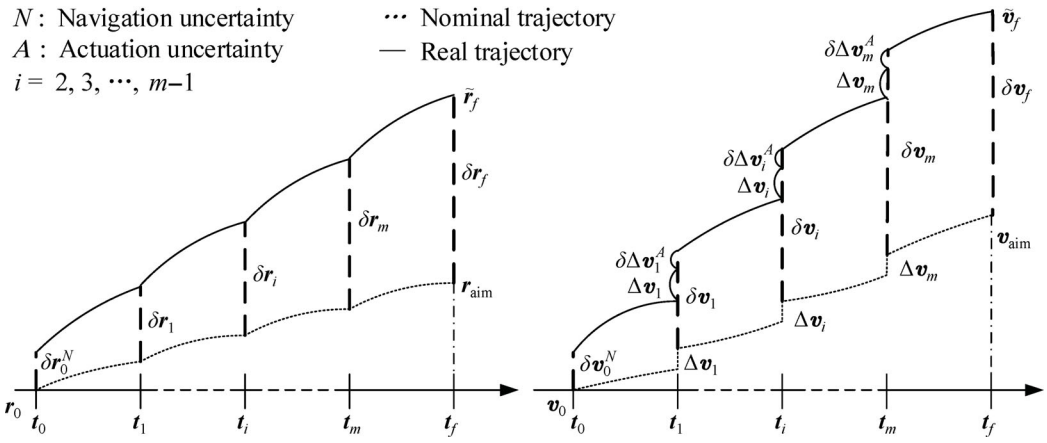

Fig. 1 Orbital uncertainty propagation process.

propagation process with multiple impulses can be described using four steps: (1) add a random realization of the navigation uncertainty $[\delta \boldsymbol{r}_0, \delta \boldsymbol{v}_0]^{\mathrm{T}}$ into the initial nominal state $[\boldsymbol{r}_0, \boldsymbol{v}_0]^{\mathrm{T}}$; (2) propagate the random realization of the real state $[\tilde{\boldsymbol{r}}_0, \tilde{\boldsymbol{v}}_0]^{\mathrm{T}}$ to the maneuver time using the governing dynamics; (3) add a random realization of the uncertain impulse $\Delta\tilde{\boldsymbol{v}}_i$ into the chaser's velocity vector; (4) repeat steps (2) and (3) until the final time and obtain the random realization of the final states $[\tilde{\boldsymbol{r}}_f, \tilde{\boldsymbol{v}}_f]^{\mathrm{T}}$.

As shown in Fig. 1, the nominal trajectory is divided into $(m+1)$ segments by the m impulses. The propagation of navigation and impulsive maneuver uncertainties can be processed piecewise using the STT-based method presented in Yang *et al.* [12]. However, this STT-based propagator can only be useful for short-term uncertainty propagations or problems with small initial uncertainty, because the Taylor approximation errors will be quickly enlarged by the STTs in different segments of the trajectory, which makes the given STTs become insufficient to approximate the solutions at the latter segments of the trajectory. To overcome this shortage, this study builds a set of modified STTs which can handle the abrupt state jumps at each maneuver time and thus directly propagate the initial uncertainty to the final time.

In this study, the following assumptions are made:

(1) The navigation uncertainty and impulsive maneuver uncertainties are Gaussian and pairwise uncorrelated. Because the impulsive maneuvers are computed based on the nominal trajectory but not intended to satisfy the terminal conditions in a closed-loop control manner, the navigation and orbital maneuvers are independent random events. Thus, the navigation and maneuver uncertainties can be assumed as independent random variables.

(2) The impulsive maneuver uncertainties are zero means. Under this assumption, most of the higher-order cross-correlated moments between navigation and maneuver uncertainties are zeros, and a simplified covariance propagation can be obtained (see the formulation in Section 4.1).

It is noted that the navigation uncertainty $\delta\boldsymbol{x}_0$ can be nonzero means, and that the components of navigation uncertainty $\delta\boldsymbol{x}_0$ or the components of a specific impulse uncertainty $\delta\Delta\boldsymbol{v}_i (i = 1, 2, \cdots, m)$ can be correlated. An intuitive understanding on this "correlated" is that the covariance matrix of $\delta\boldsymbol{x}_0$ or $\delta\Delta\boldsymbol{v}_i$ has no need to be diagonal.

The statistics of a Gaussian random vector can be completely described by the first two moments (mean and covariance matrix). Thus, only the first two moments are needed to propagate under the assumption of Gaussian distribution. However, there is no guarantee that the Gaussian distribution will remain Gaussian after propagating through a nonlinear dynamics. To solve this issue, a method of combining GMM and STT is used to approximate the PDF of the propagated uncertainty.

3 Formulation of state transition tensors

3.1 State transition tensors without maneuvers

The spacecraft's dynamics of Eq. (1) is rewritten in tensor notation:

$$\dot{\boldsymbol{x}}^i(t) = \boldsymbol{f}^i[t, \boldsymbol{x}(t)] \tag{5}$$

where $\boldsymbol{x} = \{\boldsymbol{x}^i | i = 1, \cdots, n\}$, and $n = 6$ is the dimensional size of the dynamics. For a given initial condition $\boldsymbol{x}_0 = \boldsymbol{x}(t_0)$, the solution to Eq. (7) is denoted as

$$\boldsymbol{x}(t) = \boldsymbol{\phi}(t; \boldsymbol{x}_0, t_0) \tag{6}$$

By applying the Kth order Taylor series expansion about the initial condition, the deviation of the current state from a nominal trajectory can be represented as [9]:

$$\begin{aligned}\delta\boldsymbol{x}^i(t) &= \boldsymbol{\phi}^i(t; \boldsymbol{x}_0 + \delta\boldsymbol{x}_0, t_0) - \boldsymbol{\phi}^i(t; \boldsymbol{x}_0, t_0) \\ &= \sum_{p=1}^{K} \frac{1}{p!} \boldsymbol{\Phi}^{i,k_1\cdots k_p}_{(t,t_0)} \delta\boldsymbol{x}_0^{k_1} \cdots \delta\boldsymbol{x}_0^{k_p}\end{aligned} \tag{7}$$

where the Einstein summation convention is used, and $\boldsymbol{\Phi}^{i,k_1\cdots k_p}_{(t,t_0)} = \partial^p \boldsymbol{x}^i(t)/\partial\boldsymbol{x}_0^{k_1} \cdots \partial\boldsymbol{x}_0^{k_p}$ are the STTs from t_0 to t. The STTs can be calculated by integrating the differential equation (A1) in Appendix A. As shown in Eq. (7), after the STTs are computed along the nominal trajectory, a random realization of the current state deviation $\delta\boldsymbol{x}(t)$ can be computed as an analytic function of the random initial state deviation $\delta\boldsymbol{x}_0$.

Equation (7) gives the nonlinear mapping of orbital deviation from the initial time to a future time when the nominal trajectory is consecutive. However, this consecutive mapping cannot be directly used to propagate orbital deviation when there is an abrupt state jump in the nominal trajectory, e.g., an orbital maneuver is performed. In this case, the STTs before and after a maneuver need to be connected so as to propagate the initial deviation to the final time. For the linear case, the state transition matrix (STM) $\boldsymbol{\Phi}^{i,k_1}$ is inherently transitive, thus can be directly connected as $\boldsymbol{\Phi}^{i,l_1}_{(t_f,t_0)} = \boldsymbol{\Phi}^{i,k_1}_{(t_f,t_j)} \boldsymbol{\Phi}^{k_1,l_1}_{(t_j,t_0)}$, where the superscripts i, l_1, k_1 are general indexes belonging to set $\{1, 2, \cdots, n\}$. For the nonlinear case, however, the STTs are not transitive. A method to connect the nonlinear STTs will be given in the next section.

3.2 Modified state transition tensors with maneuvers

Assuming that impulsive maneuvers $\Delta\boldsymbol{v}_i (i = 1, 2, \cdots, m)$ are executed in the propagation duration $[t_0, t_f]$. The nominal trajectory is divided into $(m+1)$ segments by these m impulses, as shown in Fig. 1. The STTs need to be computed independently for every segment after adding the impulse into the state's velocity part. If the initial navigation uncertainty is piecewise propagated to the final time using the segmented propagation in Appendix B, the propagation error will be enlarged. For example, at the time of t_0, the Taylor approximation error of Eq. (B1) is acceptable for the input parameters $\boldsymbol{m}(t_0), \boldsymbol{P}(t_0)$, as the input uncertainty is relatively small. However, at the time of t_1, the input parameters $\boldsymbol{m}(t_1), \boldsymbol{P}(t_1)$ for Eq. (B1) become larger after a nonlinear mapping from t_0 to t_1, which may result in a very large approximation error if the second-order solution of Eq. (B1) is still used. Consequently, the Taylor approximation error of Eq. (B1) will be increasingly enlarged if it is recursively used from t_0 to t_1. To avoid this problem, a set of modified STTs that can directly propagate the initial uncertainty to the final time is derived.

We first consider only one abrupt state jump existing in the nominal trajectory, i.e., to propagate the initial state error $\delta\boldsymbol{x}(t_0)$ from t_0 to t_2, during which the first impulse is performed at t_1, as shown in Fig. 1. Assuming that there is a set of modified STTs which can directly propagate the state error $\delta\boldsymbol{x}(t_0)$ from t_0 to t_2 with the similar Taylor expansions like Eq. (7):

$$\delta\boldsymbol{x}^i(t_2) = \sum_{p=1}^{K} \frac{1}{p!} \boldsymbol{\Phi}^{i,l_1\cdots l_p}_{(t_2,t_0)} \delta\boldsymbol{x}_0^{l_1} \cdots \delta\boldsymbol{x}_0^{l_p} \tag{8}$$

According to Eq. (7), the propagation of the state error in the first segment can be expressed as

$$\delta\boldsymbol{x}^{k_1}(t_1) = \sum_{q=1}^{K} \frac{1}{q!} \boldsymbol{\Phi}^{k_1,l_1\cdots l_q}_{(t_1,t_0)} \delta\boldsymbol{x}_0^{l_1} \cdots \delta\boldsymbol{x}_0^{l_q} \tag{9}$$

and the propagation of the state error in the second segment is

$$\delta\boldsymbol{x}^i(t_2) = \sum_{p=1}^{K} \frac{1}{p!} \boldsymbol{\Phi}^{i,k_1\cdots k_p}_{(t_2,t_1)} \delta\boldsymbol{x}_1^{k_1} \cdots \delta\boldsymbol{x}_1^{k_p} \tag{10}$$

where the superscripts, i, $k_1\cdots k_p$, and $l_1\cdots l_p$ are general indexes belonging to set $\{1, 2, \cdots, n\}$, and $\delta\boldsymbol{x}_j = \delta\boldsymbol{x}(t_j)$ for $j = 0, 1, 2$. It is noted that the initial conditions for computing the STTs $\boldsymbol{\Phi}^{i,k_1\cdots k_p}_{(t_2,t_1)}$ using Eq. (A1) in Appendix A are: $\boldsymbol{x}_1^+ = \boldsymbol{x}_1 + [0, 0, 0, \Delta\boldsymbol{v}_1]^{\mathrm{T}}$, $\boldsymbol{\Phi}^{i,k_1}_{(t_2,t_1)} = 1$ if $i = k_1$, and all the other elements of $\boldsymbol{\Phi}^{i,k_1\cdots k_p}_{(t_2,t_1)}$ are zero. Here the superscript "+" indicates the post-maneuver state, and x_1^+ is the initial condition for computing the higher-order partials $\boldsymbol{f}^{i,k_1\cdots k_p}(t_1)$ in Eq. (A1).

Substituting Eq. (9) into Eq. (10), the nonlinear mapping from t_0 to t_2 can be obtained as

$$\delta\boldsymbol{x}^i(t_2)=\sum_{p=1}^{K}\left[\frac{1}{p!}\boldsymbol{\Phi}^{i,k_1\cdots k_p}_{(t_2,t_1)}\left(\sum_{q=1}^{K}\frac{1}{q!}\boldsymbol{\Phi}^{k_1,l_1\cdots l_q}_{(t_1,t_0)}\delta\boldsymbol{x}_0^{l_1}\cdots\delta\boldsymbol{x}_0^{l_q}\right)\right.$$
$$\left.\cdots\left(\sum_{q=1}^{K}\frac{1}{q!}\boldsymbol{\Phi}^{k_p,l_1\cdots l_q}_{(t_1,t_0)}\delta\boldsymbol{x}_0^{l_1}\cdots\delta\boldsymbol{x}_0^{l_q}\right)\right] \tag{11}$$

Equation (11) can be expanded to any order. For example, truncating the Taylor expansions in Eq. (11) to the second order, i.e., $K=2$, we can obtain:

$$\begin{aligned}\delta\boldsymbol{x}^i(t_2)&=\boldsymbol{\Phi}^{i,k_1}_{(t_2,t_1)}\delta\boldsymbol{x}_1^{k_1}+\frac{1}{2}\boldsymbol{\Phi}^{i,k_1k_2}_{(t_2,t_1)}\delta\boldsymbol{x}_1^{k_1}\delta\boldsymbol{x}_1^{k_2}\\&=\boldsymbol{\Phi}^{i,k_1}_{(t_2,t_1)}\left(\boldsymbol{\Phi}^{k_1,l_1}_{(t_1,t_0)}\delta\boldsymbol{x}_0^{l_1}+\frac{1}{2}\boldsymbol{\Phi}^{k_1,l_1l_2}_{(t_1,t_0)}\delta\boldsymbol{x}_0^{l_1}\delta\boldsymbol{x}_0^{l_2}\right)\\&\quad+\frac{1}{2}\boldsymbol{\Phi}^{i,k_1k_2}_{(t_2,t_1)}\left(\boldsymbol{\Phi}^{k_1,l_1}_{(t_1,t_0)}\delta\boldsymbol{x}_0^{l_1}\right)\left(\boldsymbol{\Phi}^{k_2,l_2}_{(t_1,t_0)}\delta\boldsymbol{x}_0^{l_2}\right)\\&=\boldsymbol{\Phi}^{i,k_1}_{(t_2,t_1)}\boldsymbol{\Phi}^{k_1,l_1}_{(t_1,t_0)}\delta\boldsymbol{x}_0^{l_1}+\frac{1}{2}\left(\boldsymbol{\Phi}^{i,k_1}_{(t_2,t_1)}\boldsymbol{\Phi}^{k_1,l_1l_2}_{(t_1,t_0)}\right.\\&\quad\left.+\boldsymbol{\Phi}^{i,k_1k_2}_{(t_2,t_1)}\boldsymbol{\Phi}^{k_1,l_1}_{(t_1,t_0)}\boldsymbol{\Phi}^{k_2,l_2}_{(t_1,t_0)}\right)\delta\boldsymbol{x}_0^{l_1}\delta\boldsymbol{x}_0^{l_2}\end{aligned} \tag{12}$$

Comparing the same order terms in Eq. (12) with those in Eq. (8) for $K=2$, then the STTs $\boldsymbol{\Phi}^{i,l_1l_2}_{(t_2,t_0)}$ can be obtained. We further truncate Eq. (11) to the fourth order ($K=4$); after some algebra, the STTs $\boldsymbol{\Phi}^{i,l_1l_2l_3l_4}_{(t_2,t_0)}$ can be obtained as

$$\begin{aligned}\boldsymbol{\Phi}^{i,l_1}_{(t_2,t_0)}&=\boldsymbol{\Phi}^{i,k_1}_{(t_2,t_1)}\boldsymbol{\Phi}^{k_1,l_1}_{(t_1,t_0)}\\\boldsymbol{\Phi}^{i,l_1l_2}_{(t_2,t_0)}&=\boldsymbol{\Phi}^{i,k_1}_{(t_2,t_1)}\boldsymbol{\Phi}^{k_1,l_1l_2}_{(t_1,t_0)}+\boldsymbol{\Phi}^{i,k_1k_2}_{(t_2,t_1)}\boldsymbol{\Phi}^{k_1,l_1}_{(t_1,t_0)}\boldsymbol{\Phi}^{k_2,l_2}_{(t_1,t_0)}\\\boldsymbol{\Phi}^{i,l_1l_2l_3}_{(t_2,t_0)}&=\boldsymbol{\Phi}^{i,k_1}_{(t_2,t_1)}\boldsymbol{\Phi}^{k_1,l_1l_2l_3}_{(t_1,t_0)}\\&\quad+\boldsymbol{\Phi}^{i,k_1k_2k_3}_{(t_2,t_1)}\boldsymbol{\Phi}^{k_1,l_1}_{(t_1,t_0)}\boldsymbol{\Phi}^{k_2,l_2}_{(t_1,t_0)}\boldsymbol{\Phi}^{k_3,l_3}_{(t_1,t_0)}\\&\quad+1.5\boldsymbol{\Phi}^{i,k_1k_2}_{(t_2,t_1)}\boldsymbol{\Phi}^{k_1,l_1}_{(t_1,t_0)}\boldsymbol{\Phi}^{k_2,l_2l_3}_{(t_1,t_0)}\\&\quad+1.5\boldsymbol{\Phi}^{i,k_1k_2}_{(t_2,t_1)}\boldsymbol{\Phi}^{k_1,l_1l_2}_{(t_1,t_0)}\boldsymbol{\Phi}^{k_2,l_3}_{(t_1,t_0)}\\\boldsymbol{\Phi}^{i,l_1l_2l_3l_4}_{(t_2,t_0)}&=\boldsymbol{\Phi}^{i,k_1}_{(t_2,t_1)}\boldsymbol{\Phi}^{k_1,l_1l_2l_3l_4}_{(t_1,t_0)}\\&\quad+\boldsymbol{\Phi}^{i,k_1k_2k_3k_4}_{(t_2,t_1)}\boldsymbol{\Phi}^{k_1,l_1}_{(t_1,t_0)}\boldsymbol{\Phi}^{k_2,l_2}_{(t_1,t_0)}\boldsymbol{\Phi}^{k_3,l_3}_{(t_1,t_0)}\boldsymbol{\Phi}^{k_4,l_4}_{(t_1,t_0)}\\&\quad+2\boldsymbol{\Phi}^{i,k_1k_2}_{(t_2,t_1)}\boldsymbol{\Phi}^{k_1,l_1}_{(t_1,t_0)}\boldsymbol{\Phi}^{k_2,l_2l_3l_4}_{(t_1,t_0)}\\&\quad+3\boldsymbol{\Phi}^{i,k_1k_2}_{(t_2,t_1)}\boldsymbol{\Phi}^{k_1,l_1l_2}_{(t_1,t_0)}\boldsymbol{\Phi}^{k_2,l_3l_4}_{(t_1,t_0)}\\&\quad+2\boldsymbol{\Phi}^{i,k_1k_2}_{(t_2,t_1)}\boldsymbol{\Phi}^{k_1,l_1l_2l_3}_{(t_1,t_0)}\boldsymbol{\Phi}^{k_2,l_4}_{(t_1,t_0)}\\&\quad+2\boldsymbol{\Phi}^{i,k_1k_2k_3}_{(t_2,t_1)}\boldsymbol{\Phi}^{k_1,l_1}_{(t_1,t_0)}\boldsymbol{\Phi}^{k_2,l_2l_3}_{(t_1,t_0)}\boldsymbol{\Phi}^{k_3,l_4}_{(t_1,t_0)}\\&\quad+2\boldsymbol{\Phi}^{i,k_1k_2k_3}_{(t_2,t_1)}\boldsymbol{\Phi}^{k_1,l_1l_2}_{(t_1,t_0)}\boldsymbol{\Phi}^{k_2,l_3}_{(t_1,t_0)}\boldsymbol{\Phi}^{k_3,l_4}_{(t_1,t_0)}\\&\quad+2\boldsymbol{\Phi}^{i,k_1k_2k_3}_{(t_2,t_1)}\boldsymbol{\Phi}^{k_1,l_1}_{(t_1,t_0)}\boldsymbol{\Phi}^{k_2,l_2}_{(t_1,t_0)}\boldsymbol{\Phi}^{k_3,l_3l_4}_{(t_1,t_0)}\end{aligned} \tag{13}$$

Once the STTs $\boldsymbol{\Phi}^{i,l_1\cdots l_4}_{(t_2,t_0)}$ are calculated using Eq. (13), the initial state error $\delta\boldsymbol{x}_0$ can be directly propagated to time t_2 using Eq. (8). For the cases with multiple impulses $\Delta\boldsymbol{v}_j(j=1,2,\cdots,m)$, Eq. (13) can be recursively applied to the following segmented trajectory ($j=3,4,\cdots,m$). For instance, replacing $\boldsymbol{\Phi}^{i,k_1\cdots k_p}_{(t_2,t_1)}$ and $\boldsymbol{\Phi}^{k_i,l_1\cdots l_p}_{(t_1,t_0)}$ with $\boldsymbol{\Phi}^{i,k_1\cdots k_p}_{(t_3,t_2)}$ and $\boldsymbol{\Phi}^{k_i,l_1\cdots l_p}_{(t_2,t_0)}$, respectively, then the STTs $\boldsymbol{\Phi}^{i,l_1\cdots l_p}_{(t_3,t_0)}$ can be computed using Eq. (13). It is noted that the modified STTs in Eq. (13) is a connection of the regular STTs in different segments of the nominal trajectory. At the beginning of each trajectory, the nominal state is replaced by the new state after the impulsive maneuver.

Finally, the propagation of state error from the time $t_j(j=0,1,\cdots,m)$ to the final time t_f using the modified STTs $\boldsymbol{\Phi}^{i,l_1\cdots l_4}_{(t_f,t_j)}$ can be obtained as

$$\delta\boldsymbol{x}^i(t_f)=\sum_{p=1}^{4}\frac{1}{p!}\boldsymbol{\Phi}^{i,l_1\cdots l_p}_{(t_f,t_j)}\delta\boldsymbol{x}_j^{l_1}\cdots\delta\boldsymbol{x}_j^{l_p} \tag{14}$$

4 Uncertainty propagation methods

The STTs can be used to analytically propagate the statistical moments of initial state uncertainty, e.g., mean and covariance matrix [9, 10]. They can also be used to propagate the PDF of the initial state uncertainty by combining with a GMM method [30]. However, the propagation of impulsive maneuver uncertainties using STTs was not given in previous studies. This section considers the analytical propagation of the initial state uncertainty and the impulsive maneuver uncertainty using the modified STTs.

4.1 Nonlinear covariance propagation

4.1.1 Covariance propagation of initial state uncertainty

According to the fundamental theories of probability, the mean and covariance matrix of a random vector $\delta\boldsymbol{x}$ are defined as

$$\begin{aligned}\boldsymbol{m}^i&=E[\delta\boldsymbol{x}^i]\\\boldsymbol{P}^{ij}&=E[(\delta\boldsymbol{x}^i-\boldsymbol{m}^i)(\delta\boldsymbol{x}^j-\boldsymbol{m}^j)]\\&=E[\delta\boldsymbol{x}^i\delta\boldsymbol{x}^j]-\boldsymbol{m}^i\boldsymbol{m}^j\end{aligned} \tag{15}$$

where $E[\cdot]$ represents the expectation operator.

The propagation of mean and covariance matrix can be obtained by substituting Eq. (14) into Eq. (15). The

method of unfolding Eq. (15) is the same for any value of K in Eq. (14). However, the mathematic expressions are quite complicate for a big K. For simplicity, we illustratively unfold Eq. (15) by truncating Eq. (14) to the second order ($K=2$). After some algebra, the first two moments can be expressed as

$$\begin{aligned}\boldsymbol{m}^i(t_f)&=\boldsymbol{\Phi}^{i,a}_{(t_f,t_0)}E[\delta\boldsymbol{x}^a_0]+\frac{1}{2}\boldsymbol{\Phi}^{i,ab}_{(t_f,t_0)}E[\delta\boldsymbol{x}^a_0\delta\boldsymbol{x}^b_0]\\ \boldsymbol{P}^{ij}(t_f)&=\boldsymbol{\Phi}^{i,a}_{(t_f,t_0)}\boldsymbol{\Phi}^{j,b}_{(t_f,t_0)}E[\delta\boldsymbol{x}^a_0\delta\boldsymbol{x}^b_0]\\ &\quad+\frac{1}{4}\boldsymbol{\Phi}^{i,ab}_{(t_f,t_0)}\boldsymbol{\Phi}^{j,cd}_{(t_f,t_0)}E[\delta\boldsymbol{x}^a_0\delta\boldsymbol{x}^b_0\delta\boldsymbol{x}^c_0\delta\boldsymbol{x}^d_0]\\ &\quad+\frac{1}{2}\left[\boldsymbol{\Phi}^{i,a}_{(t_f,t_0)}\boldsymbol{\Phi}^{j,bc}_{(t_f,t_0)}+\boldsymbol{\Phi}^{j,a}_{(t_f,t_0)}\boldsymbol{\Phi}^{i,bc}_{(t_f,t_0)}\right]\\ &\quad\cdot E[\delta\boldsymbol{x}^a_0\delta\boldsymbol{x}^b_0\delta\boldsymbol{x}^c_0]-\boldsymbol{m}^i_f\boldsymbol{m}^j_f\end{aligned}\tag{16}$$

For the Gaussian distribution, its third and fourth raw moments can be computed using the mean and covariance matrix [9]:

$$\begin{aligned}&E[\delta\boldsymbol{x}^a_0]=\boldsymbol{m}^a_0\\ &E[\delta\boldsymbol{x}^a_0\delta\boldsymbol{x}^b_0]=\boldsymbol{P}^{ab}_0+\boldsymbol{m}^a_0\boldsymbol{m}^b_0\\ &E[\delta\boldsymbol{x}^a_0\delta\boldsymbol{x}^b_0\delta\boldsymbol{x}^c_0]=\boldsymbol{m}^a_0\boldsymbol{m}^b_0\boldsymbol{m}^c_0+\boldsymbol{m}^a_0\boldsymbol{P}^{bc}_0+\boldsymbol{m}^b_0\boldsymbol{P}^{ac}_0+\boldsymbol{m}^c_0\boldsymbol{P}^{ab}_0\\ &E[\delta\boldsymbol{x}^a_0\delta\boldsymbol{x}^b_0\delta\boldsymbol{x}^c_0\delta\boldsymbol{x}^d_0]=\boldsymbol{m}^a_0\boldsymbol{m}^b_0\boldsymbol{m}^c_0\boldsymbol{m}^d_0+\boldsymbol{P}^{ab}_0\boldsymbol{P}^{cd}_0\\ &\qquad+\boldsymbol{P}^{ac}_0\boldsymbol{P}^{bd}_0+\boldsymbol{P}^{ad}_0\boldsymbol{P}^{bc}_0+\boldsymbol{m}^a_0\boldsymbol{m}^b_0\boldsymbol{P}^{cd}_0\\ &\qquad+\boldsymbol{m}^a_0\boldsymbol{m}^c_0\boldsymbol{P}^{bd}_0+\boldsymbol{m}^a_0\boldsymbol{m}^d_0\boldsymbol{P}^{bc}_0\\ &\qquad+\boldsymbol{m}^b_0\boldsymbol{m}^c_0\boldsymbol{P}^{ad}_0+\boldsymbol{m}^b_0\boldsymbol{m}^d_0\boldsymbol{P}^{ac}_0\\ &\qquad+\boldsymbol{m}^c_0\boldsymbol{m}^d_0\boldsymbol{P}^{ab}_0\end{aligned}\tag{17}$$

It is noted that the 6th or 8th raw moments need to be computed for the respective value of $K=3$ or $K=4$ in Eq. (14). A method to compute the higher-order raw moments can be found in Phillips [35]. For the sake of convenience, the nonlinear uncertainty propagation in Eqs. (16) and (17) is denoted as

$$[\boldsymbol{m}_f,\boldsymbol{P}_f]=STT\left[t_f;t_0,\boldsymbol{m}_0,\boldsymbol{P}_0,\boldsymbol{\Phi}^{i,k_1k_2}_{(t_f,t_0)}\right]\tag{18}$$

4.1.2 Covariance propagation of impulsive maneuver uncertainties

Equation (18) can be used to propagate the initial state uncertainty. However, the uncertainties on impulsive maneuvers are not included in Eq. (18). This section formulates the analytical propagation of impulsive maneuver uncertainties.

We denote a random realization of the jth impulsive maneuver uncertainty as $\delta\Delta\boldsymbol{v}_j$, then the post-maneuver orbital uncertainty at t_j can be expressed as

$$\begin{aligned}&\delta\boldsymbol{x}^+_j=\delta\boldsymbol{x}_j+\delta\boldsymbol{x}_{vj},\ \ j=1,2,\cdots,m\\ &\delta\boldsymbol{x}_j=\delta\boldsymbol{x}(t_j),\ \ \delta\boldsymbol{x}_{vj}=\boldsymbol{R}\delta\Delta\boldsymbol{v}_j\end{aligned}\tag{19}$$

where $\Delta\boldsymbol{v}_j$ is the jth nominal impulse, $\delta\boldsymbol{x}_{vj}$ is a random realization of the state uncertainty caused by the jth impulse, $\delta\boldsymbol{x}(t_j)$ is a random realization of the state uncertainty that is propagated from $\delta\boldsymbol{x}^+(t_{j-1})$, $\boldsymbol{R}=[\boldsymbol{0}_3,\boldsymbol{I}_3]^{\mathrm{T}}$ is the (6×3)-dimensional mapping matrix from pure velocity space to the combined position and velocity space, and $\boldsymbol{I}$ denotes the identical matrix.

For clarity, we first consider only one maneuver, i.e., $m=1$. Substituting Eq. (19) into Eq. (14) and truncating the Taylor expansions to the second order ($K=2$), then the final state error can be expressed as

$$\begin{aligned}\delta\boldsymbol{x}^i(t_f)&=\boldsymbol{\Phi}^{i,k_1}_{(t_f,t_1)}(\delta\boldsymbol{x}^{k_1}_1+\delta\boldsymbol{x}^{k_1}_{v1})\\ &\quad+\frac{1}{2}\boldsymbol{\Phi}^{i,k_1k_2}_{(t_f,t_1)}(\delta\boldsymbol{x}^{k_1}_1+\delta\boldsymbol{x}^{k_1}_{v1})(\delta\boldsymbol{x}^{k_2}_1+\delta\boldsymbol{x}^{k_2}_{v1})\end{aligned}\tag{20}$$

Substituting Eq. (9) into Eq. (20), then the following equations can be obtained:

$$\begin{aligned}\delta\boldsymbol{x}^i(t_f)&=\mathrm{d}A+\mathrm{d}B+\mathrm{d}C\\ \mathrm{d}A&=\boldsymbol{\Phi}^{i,k_1}_{(t_f,t_0)}\delta\boldsymbol{x}^{k_1}_0+\frac{1}{2}\boldsymbol{\Phi}^{i,k_1k_2}_{(t_f,t_0)}\delta\boldsymbol{x}^{k_1}_0\delta\boldsymbol{x}^{k_2}_0\\ \mathrm{d}B&=\boldsymbol{\Phi}^{i,k_1}_{(t_f,t_1)}\delta\boldsymbol{x}^{k_1}_{v1}+\frac{1}{2}\boldsymbol{\Phi}^{i,k_1k_2}_{(t_f,t_1)}\delta\boldsymbol{x}^{k_1}_{v1}\delta\boldsymbol{x}^{k_2}_{v1}\\ \mathrm{d}C&=\boldsymbol{\Phi}^{i,l_1l_2}_{(t_f,t_1)}\boldsymbol{\Phi}^{l_1,k_1}_{(t_1,t_0)}\boldsymbol{I}^{l_2,k_2}_6\delta\boldsymbol{x}^{k_1}_0\delta\boldsymbol{x}^{k_2}_{v1}\end{aligned}\tag{21}$$

Similarly, the concept of deriving Eq. (21) can be recursively applied to the cases with multiple impulses $\Delta\boldsymbol{v}_j(j=1,2,\cdots,m)$. Therefore, the final state error $\delta\boldsymbol{x}(t_f)$ can be expressed as a nonlinear mapping of the initial state error $\delta\boldsymbol{x}(t_0)$ and the state error $\delta\boldsymbol{x}_{vj}$ caused by the impulsive maneuvers, i.e.

$$\begin{aligned}\delta\boldsymbol{x}^i_f&=\boldsymbol{\Phi}^{i,k_1}_{(t_f,t_0)}\delta\boldsymbol{x}^{k_1}_0+\frac{1}{2}\boldsymbol{\Phi}^{i,k_1k_2}_{(t_f,t_0)}\delta\boldsymbol{x}^{k_1}_0\delta\boldsymbol{x}^{k_2}_0\\ &\quad+\sum_{j=1}^{m}\left(\boldsymbol{\Phi}^{i,k_1}_{(t_f,t_j)}\delta\boldsymbol{x}^{k_1}_{vj}+\frac{1}{2}\boldsymbol{\Phi}^{i,k_1k_2}_{(t_f,t_j)}\delta\boldsymbol{x}^{k_1}_{vj}\delta\boldsymbol{x}^{k_2}_{vj}\right)\\ &\quad+\sum_{j=1}^{m}\left(\boldsymbol{\Theta}^{i,k_1k_2}_{(t_f,t_j,t_0)}\delta\boldsymbol{x}^{k_1}_0\delta\boldsymbol{x}^{k_2}_{vj}\right)\\ &\quad+\sum_{j=1}^{m-1}\sum_{n=j+1}^{m}\left(\boldsymbol{\Theta}^{i,k_1k_2}_{(t_f,t_n,t_j)}\delta\boldsymbol{x}^{k_1}_{vn}\delta\boldsymbol{x}^{k_2}_{vj}\right)\end{aligned}\tag{22}$$

where for $k=0,1,\cdots,m$, the modified STTs $\boldsymbol{\Phi}^{i,k_1k_2}_{(t_f,t_j)}$ are computed using Eq. (13), and the modified STTs related to the impulsive maneuver uncertainties can be

expressed as

$$\begin{aligned}\boldsymbol{\Theta}^{i,k_1k_2}_{(t_f,t_j,t_0)} &= \boldsymbol{\Phi}^{i,l_1l_2}_{(t_f,t_j)}\boldsymbol{\Phi}^{l_1,k_1}_{(t_j,t_0)}\boldsymbol{I}^{l_2,k_2}_6\\ \boldsymbol{\Theta}^{i,k_1k_2}_{(t_f,t_n,t_j)} &= \boldsymbol{\Phi}^{i,l_1l_2}_{(t_f,t_n)}\boldsymbol{\Phi}^{l_1,k_1}_{(t_n,t_j)}\boldsymbol{I}^{l_2,k_2}_6\end{aligned} \tag{23}$$

Based on the assumptions given in Section 2.3, the initial navigation uncertainty and the impulsive maneuver uncertainties are pairwise independent random variables, thus most of the cross-correlated moments such as $E[\delta\boldsymbol{x}_0\delta\boldsymbol{x}_{vj}]$, $E[\delta\boldsymbol{x}_0\delta\boldsymbol{x}_0\delta\boldsymbol{x}_{vj}]$, $E[\delta\boldsymbol{x}_0\delta\boldsymbol{x}_0\delta\boldsymbol{x}_0\delta\boldsymbol{x}_{vj}]$, and $E[\delta\boldsymbol{x}_0\delta\boldsymbol{x}_{vj}\delta\boldsymbol{x}_{vj}\delta\boldsymbol{x}_{vj}]$ are zeros. However, the cross-correlated terms $E[\delta\boldsymbol{x}_0\delta\boldsymbol{x}_{vj}\delta\boldsymbol{x}_{vj}]$, $E[\delta\boldsymbol{x}_0\delta\boldsymbol{x}_0\delta\boldsymbol{x}_{vj}\delta\boldsymbol{x}_{vj}]$, and $E[\delta\boldsymbol{x}_{vn}\delta\boldsymbol{x}_{vn}\delta\boldsymbol{x}_{vj}\delta\boldsymbol{x}_{vj}]$ are nonzero. Substituting Eq. (22) into Eq. (15) and truncating the Taylor series to the second order, then the mean $\boldsymbol{m}_f$ and covariance matrix $\boldsymbol{P}_f$ of the final state uncertainty can be obtained as

$$\begin{aligned}&\boldsymbol{m}_f = \boldsymbol{m}_f^{(1)}, \quad \boldsymbol{P}_f = \boldsymbol{P}_f^{(1)} + \boldsymbol{P}_f^{(2)} + \boldsymbol{P}_f^{(3)} + \boldsymbol{P}_f^{(4)}\\ &\left[\boldsymbol{m}_f^{(1)}, \boldsymbol{P}_f^{(1)}\right] = STT\left[t_f; t_0, \boldsymbol{m}_0, \boldsymbol{P}_0, \boldsymbol{\Phi}^{k_1k_2}_{(t_f,t_0)}\right]\\ &\qquad + \sum_{j=1}^{m} STT\left[t_f; t_j, \boldsymbol{m}_{vj}, \boldsymbol{P}_{vj}, \boldsymbol{\Phi}^{k_1k_2}_{(t_f,t_j)}\right]\end{aligned} \tag{24}$$

where $j = 1, \cdots, m$, and the similar denotation like Eq. (18) is applied to describe the propagation of impulsive maneuver uncertainties. Denoting the mean and covariance matrix of the jth impulse uncertainty as $E[\delta\Delta\boldsymbol{v}_j]$ and $\boldsymbol{P}(\delta\Delta\boldsymbol{v}_j)$, respectively, then $\boldsymbol{m}_{vj} = \boldsymbol{R}\times E[\delta\Delta\boldsymbol{v}_j]$ and $\boldsymbol{P}_{vj} = \boldsymbol{R}\times\boldsymbol{P}(\delta\Delta\boldsymbol{v}_j)\times\boldsymbol{R}^{\mathrm{T}}$. Under the assumption of Gaussian distribution, the third and fourth moments of $\delta\boldsymbol{x}_{vj}$ can be computed by substituting $\boldsymbol{m}_{vj}$ and $\boldsymbol{P}_{vj}$ into Eq. (17), and the expressions of $\boldsymbol{P}_f^{(2)}$, $\boldsymbol{P}_f^{(3)}$, and $\boldsymbol{P}_f^{(4)}$ are

$$\begin{aligned}\left[\boldsymbol{P}_f^{(2)}\right]^{ij} &= \sum_{k=1}^{m}\left(\boldsymbol{\Phi}^{i,l_1}_{(t_f,t_k)}\boldsymbol{\Theta}^{j,l_2l_3}_{(t_f,t_k,t_0)} + \boldsymbol{\Phi}^{j,l_1}_{(t_f,t_k)}\boldsymbol{\Theta}^{i,l_2l_3}_{(t_f,t_k,t_0)}\right)\\ &\quad\cdot E\left[\delta\boldsymbol{x}_0^{l_2}\delta\boldsymbol{x}_{vk}^{l_1}\delta\boldsymbol{x}_{vk}^{l_3}\right]\\ &\quad+\sum_{k=1}^{m}\frac{1}{2}\left(\boldsymbol{\Phi}^{i,l_1}_{(t_f,t_0)}\boldsymbol{\Phi}^{j,l_1l_2}_{(t_f,t_k)} + \boldsymbol{\Phi}^{j,l_1}_{(t_f,t_0)}\boldsymbol{\Phi}^{i,l_1l_2}_{(t_f,t_k)}\right)\\ &\quad\cdot E\left[\delta\boldsymbol{x}_0^{l_1}\delta\boldsymbol{x}_{vk}^{l_2}\delta\boldsymbol{x}_{vk}^{l_3}\right]\\ \left[\boldsymbol{P}_f^{(3)}\right]^{ij} &= \sum_{k=1}^{m}\boldsymbol{\Theta}^{i,l_1l_2}_{(t_f,t_k,t_0)}\boldsymbol{\Theta}^{j,l_3l_4}_{(t_f,t_k,t_0)}\\ &\quad\cdot E\left[\delta\boldsymbol{x}_0^{l_1}\delta\boldsymbol{x}_0^{l_3}\delta\boldsymbol{x}_{vk}^{l_2}\delta\boldsymbol{x}_{vk}^{l_4}\right]\\ &\quad+\sum_{k=1}^{m}\frac{1}{4}\left(\boldsymbol{\Phi}^{i,l_1l_2}_{(t_f,t_0)}\boldsymbol{\Phi}^{j,l_3l_4}_{(t_f,t_k)} + \boldsymbol{\Phi}^{j,l_1l_2}_{(t_f,t_0)}\boldsymbol{\Phi}^{i,l_3l_4}_{(t_f,t_k)}\right)\\ &\quad\cdot E\left[\delta\boldsymbol{x}_0^{l_1}\delta\boldsymbol{x}_0^{l_2}\delta\boldsymbol{x}_{vk}^{l_3}\delta\boldsymbol{x}_{vk}^{l_4}\right]\end{aligned}$$

$$\begin{aligned}\left[\boldsymbol{P}_f^{(4)}\right]^{ij} &= \sum_{k=1}^{m-1}\sum_{n=k+1}^{m}\boldsymbol{\Theta}^{i,l_1l_2}_{(t_f,t_n,t_k)}\boldsymbol{\Theta}^{j,l_3l_4}_{(t_f,t_n,t_k)}\\ &\quad\cdot E\left[\delta\boldsymbol{x}_{vn}^{l_1}\delta\boldsymbol{x}_{vn}^{l_3}\delta\boldsymbol{x}_{vk}^{l_2}\delta\boldsymbol{x}_{vk}^{l_4}\right]\end{aligned} \tag{25}$$

Here, the STTs $\boldsymbol{\Theta}_{(t_f,t_k,t_0)}$ and $\boldsymbol{\Theta}^{j,l_3l_4}_{(t_f,t_n,t_k)}$ are calculated using Eq. (23), and the three nonzero cross-correlated moments are

$$\begin{aligned}&E\left[\delta\boldsymbol{x}_0^{l_1}\delta\boldsymbol{x}_{vk}^{l_2}\delta\boldsymbol{x}_{vk}^{l_3}\right] = \boldsymbol{m}_0^{l_1}\boldsymbol{P}_{vk}^{l_2l_3}\\ &E\left[\delta\boldsymbol{x}_0^{l_1}\delta\boldsymbol{x}_0^{l_2}\delta\boldsymbol{x}_{vk}^{l_3}\delta\boldsymbol{x}_{vk}^{l_4}\right] = \left(\boldsymbol{m}_0^{l_1}\boldsymbol{m}_0^{l_2} + \boldsymbol{P}_0^{l_1l_2}\right)\boldsymbol{P}_{vk}^{l_3l_4}\\ &E\left[\delta\boldsymbol{x}_{vn}^{l_1}\delta\boldsymbol{x}_{vn}^{l_3}\delta\boldsymbol{x}_{vk}^{l_2}\delta\boldsymbol{x}_{vk}^{l_4}\right] = \boldsymbol{P}_{vn}^{l_1l_3}\boldsymbol{P}_{vk}^{l_2l_4}\end{aligned} \tag{26}$$

Equation (24) can be used to nonlinearly propagate the mean and covariance matrix of the initial navigation uncertainty and impulsive maneuver uncertainties. However, there is no guarantee that the Gaussian distribution will remain Gaussian after a nonlinear mapping. For a non-Gaussian distribution, the first two moments (mean and covariance) are insufficient to fully describe its PDF. In this section, a method of combining the GMM and STT (GMM_STT) is proposed to predict the PDF of a non-Gaussian distribution.

4.2 Nonlinear propagation of probability density function

The main idea of GMM approach is to approximate an arbitrary PDF by a finite sum of weighted Gaussian density functions, where the weights of different components of a GMM are determined by numerical optimization techniques, i.e.,

$$\hat{p}\left(t,\boldsymbol{x}\right) = \sum_{i=1}^{L}\boldsymbol{\omega}_i p_{\mathrm{g}}\left(\boldsymbol{x};\boldsymbol{m}_i,\boldsymbol{P}_i\right) \tag{27}$$

where L is the total number of Gaussian kernels, $\boldsymbol{m}_i$ and $\boldsymbol{P}_i$ represent the mean and covariance matrix of the ith Gaussian density function $p_{\mathrm{g}}\left(\boldsymbol{x};\boldsymbol{m}_i,\boldsymbol{P}_i\right)$, respectively; $\boldsymbol{\omega}_i$ denotes the weight of the ith Gaussian kernel. The positivity and normalization requirements on $\hat{p}\left(t,\boldsymbol{x}\right)$ lead to the following constraints:

$$\sum_{i=1}^{L}\boldsymbol{\omega}_i = 1; \quad \boldsymbol{\omega}_i \geqslant 0, \quad i = 1, \cdots, L \tag{28}$$

Theoretically, the mixture PDF, $\hat{p}\left(t,\boldsymbol{x}\right)$, approximates to the real PDF $p\left(t,\boldsymbol{x}\right)$ by increasing the number of mixtures, L. In order to obtain the final GMM, it needs to split the input uncertainty (including navigation and maneuver uncertainties) into L Gaussian

mixtures, and then to propagate every Gaussian mixture to the final time using the STT-based method, i.e., Eq. (24). The weights updating during the propagation process is not considered in this study, readers with an interest on this topic can refer to Terejanu *et al.* [36].

There are several methods available to split the initial Gaussian distribution into a GMM [26–29], and this study employs the splitting method proposed by Vittaldev and Russell [29]. This method first splits a univariate Gaussian distribution into homoscedastic components, and then extends to the multivariate case using an eigenvalue decomposition. An advantage of this method is that the splitting of a univariate Gaussian distribution can be done offline. Vittaldev and Russell provided a univariate spliting library data which can be directly applied to split a multivariate Gaussian distribution. Once the weights and moments of the L Gaussian mixtures are determined, the non-Gaussian PDF can be computed using Eq. (27), and the mean and covariance matrix can be merged as follows [27]:

$$\begin{aligned} \boldsymbol{m}_m &= \sum_{i=1}^{L} \frac{\boldsymbol{\omega}_i}{\omega_m} \boldsymbol{m}_i, \quad \omega_m = \sum_{i=1}^{L} \boldsymbol{\omega}_i \\ \boldsymbol{P}_m &= \sum_{i=1}^{L} \frac{\boldsymbol{\omega}_i}{\omega_m} \left(\boldsymbol{P}_i + \boldsymbol{m}_i \boldsymbol{m}_i^{\mathrm{T}} \right) - \boldsymbol{m}_m \boldsymbol{m}_m^{\mathrm{T}} \end{aligned} \tag{29}$$

In order to split the input uncertainty into Gaussian mixtures, the navigation and maneuver uncertainties need to be combined together as an extended state vector. The uncertainty propagation using the combined GMM and STT method is summarized as follows.

Step 1: Combine the navigation and maneuver uncertainties together as an extended, $(n + 3m)$-dimensional state: $\boldsymbol{X} = [\delta \boldsymbol{x}_0, \delta \Delta \boldsymbol{v}_1, \cdots, \delta \Delta \boldsymbol{v}_m]$. Because the random variables $\delta \boldsymbol{x}_0$ and $\delta \Delta \boldsymbol{v}_j (j = 1, \cdots, m)$ are pairwise independent with each other, then the mean and covariance matrix of the input uncertainty vector $\boldsymbol{X}$ can be expressed as

$$\begin{aligned} \bar{\boldsymbol{m}}(t_0) &= [\boldsymbol{m}(t_0), E[\delta \Delta \boldsymbol{v}_1], \cdots, E[\delta \Delta \boldsymbol{v}_m]]^{\mathrm{T}} \\ \bar{\boldsymbol{P}}(t_0) &= \begin{bmatrix} \boldsymbol{P}(t_0) & \boldsymbol{0}_{6\times 3} & \cdots & \boldsymbol{0}_{6\times 3} \\ \boldsymbol{0}_{3\times 6} & \boldsymbol{P}(\delta \Delta \boldsymbol{v}_1) & \boldsymbol{0}_{3\times 3} & \vdots \\ \vdots & \boldsymbol{0}_{3\times 3} & \ddots & \boldsymbol{0}_{3\times 3} \\ \boldsymbol{0}_{3\times 6} & \cdots & \boldsymbol{0}_{3\times 3} & \boldsymbol{P}(\delta \Delta \boldsymbol{v}_m) \end{bmatrix} \end{aligned} \tag{30}$$

Step 2: Split the multivariate Gaussian distribution $p_{\mathrm{g}}\left(\boldsymbol{x}; \bar{\boldsymbol{m}}(t_0), \bar{\boldsymbol{P}}(t_0)\right)$ into L Gaussian mixtures $\left(\boldsymbol{\omega}_i, \bar{\boldsymbol{m}}_i, \bar{\boldsymbol{P}}_i\right)(i = 1, 2, \cdots, L)$ using the splitting method proposed by Vittaldev and Russell [29]. It is noted that the input Gaussian distribution is split along the radial position in this study, because the orbital nonlinearity is more evident in radial position or transverse velocity according to Junkins and Singla [7].

Step 3: Extract the input statistical moments, i.e., $\boldsymbol{m}_i(t_0)$, $\boldsymbol{P}_i(t_0)$, $E[\delta \Delta \boldsymbol{v}_j]_i$, and $\boldsymbol{P}_i(\delta \Delta \boldsymbol{v}_j)(i = 1, 2, \cdots, L, j = 1, 2, \cdots, m)$, from the split Gaussian mixtures $\left(\bar{\boldsymbol{m}}_i, \bar{\boldsymbol{P}}_i\right)$. Propagate these moments to the final time using the modified STTs, as given by Eq. (24), then the moments $[\boldsymbol{m}_i(t_f), \boldsymbol{P}_i(t_f)]$ of final state uncertainty for every Gaussian mixture can be obtained. It is noted that the modified STTs in Eq. (13) only need to be integrated once for propagating all the Gaussian mixtures.

Step 4: Compute the PDF and moments of the final state uncertainty using Eqs. (27) and (29), respectively.

As shown in Eq. (30), the input navigation and maneuver uncertainties have a dimensionality of $(n+3m)$. For instance, the dimensionality becomes 18 if four maneuvers $(n = 6, m = 4)$ are executed, which may lead to the curse of dimensionality for some nonlinear uncertainty propagation methods, e.g., the PC expansions. However, with the method given in this study, there is no dimensionality problem and the PDF of output uncertainty can be efficiently propagated.

5 Simulation results

The rendezvous and docking mission can be divided into a number of major phases: launching, phasing, far range rendezvous (homing), close range rendezvous, and mating [34]. Most of the practical rendezvous-phasing missions last from one day to three days, and the chaser performs 4 or 5 maneuvers to acquire the "initial aim point", where the chaser can be controlled automatically by the onboard system and the far range rendezvous can begin. Generally, the chaser cannot precisely reach the initial aim point after phasing maneuvers because of uncertainties. The phasing orbital precision determines when and where to switch the ground control to onboard autonomous control, and then affects the far range rendezvous scheme design. Therefore, accurate uncertainty quantification of phasing orbits plays an important role in practical rendezvous mission design.

A near-Earth perturbed rendezvous-phasing mission is employed to validate the proposed uncertainty propagation method. The target runs on a 340 km near-circular orbit with an inclination of 42.9°, and the chaser's insertion perigee and apogee altitudes are 200

and 330 km, respectively. Their initial orbital elements (semi-major axis, eccentricity, inclination, right ascension of the ascending node, argument of periapsis, and true anomaly) are $\boldsymbol{E}_{\rm tar}(t_0)$ = [6716.3 km, 0.0006, 42.8545°, 55.7517°, 185.488°, 0°] and $\boldsymbol{E}_{\rm cha}(t_0)$ = [6636.004 km, 0.0098, 42.8376°, 55.9165°, 125.488°, 0°], respectively. The initial and final time is $t_0 = 0$ s and $t_f = 86400$ s, respectively. The coefficient of drag is $C_{\rm D} = 2.2$, the target and chaser's cross-sectional areas are $S_{\rm tar} = 30$ m^2 and $S_{\rm cha} = 20$ m^2, respectively, and their masses are $M_{\rm tar} = 8000$ kg and $M_{\rm cha} = 7500$ kg, respectively. The aimed final relative position and velocity between the chaser and target are $\boldsymbol{\rho}_{\rm aim} = [-13.5,\ -50.0,\ 0]^{\rm T}$ (km) and $\dot{\boldsymbol{\rho}}_{\rm aim} = [0,\ 23.23,\ 0]^{\rm T}$ (m/s), respectively.

Four impulsive maneuvers are executed to ensure that the chaser arrives at the aimed point at the final time of the rendezvous phasing, and the nominal impulses are listed in Table 1, which are planned based on the chaser's state $\boldsymbol{E}_{\rm cha}(t_0)$, the target's state $\boldsymbol{E}_{\rm tar}(t_f)$, and the aimed relative state $[\boldsymbol{\rho}_{\rm aim}, \dot{\boldsymbol{\rho}}_{\rm aim}]^{\rm T}$ using the method in Yang *et al.* [37]. In this study, only the chaser's navigation and maneuver uncertainties are propagated. All means and standard deviations are described in the chaser's local vertical/local horizontal (LVLH) frame, where the origin is located at the chaser's center of mass, the x-axis is along the position vector, the z-axis is along the orbit normal, and the y-axis completes the right-handed system.

The number of MC samples is 100,000. The input navigation and maneuver uncertainties are assumed as Gaussian distribution with zero means. The standard deviations for navigation uncertainty in Eq. (3) are: $\boldsymbol{\sigma}_{\delta\boldsymbol{x}} = [\boldsymbol{\sigma}_{\delta\boldsymbol{r}}, \boldsymbol{\sigma}_{\delta\boldsymbol{v}}]^{\rm T} = [100$ m, 100 m, 100 m, 0.1 m/s, 0.1 m/s, 0.1 m/s$]^{\rm T}$. The coefficients for the standard deviation of maneuver uncertainty in Eq. (4) are: $\alpha = 0.001$ and $\beta = 0.02$. The covariance matrices $\boldsymbol{P}(t_0)$ and $\boldsymbol{P}(\delta\Delta\boldsymbol{v}_j)$ in Eq. (30) are set as

$$\begin{aligned}
\boldsymbol{P}^{ij}(t_0) &= \begin{cases} \left(\sigma^i_{\delta\boldsymbol{x}}\right)^2, & i = j \\ -0.01\sigma^i_{\delta\boldsymbol{x}}\sigma^j_{\delta\boldsymbol{x}}, & i \neq j \end{cases} \\
\boldsymbol{P}^{ab}(\delta\Delta\boldsymbol{v}_k) &= \begin{cases} \left[\sigma_a(\delta\Delta\boldsymbol{v}_k)\right]^2, & a = b \\ 0.01\sigma_a(\delta\Delta\boldsymbol{v}_k)\sigma_b(\delta\Delta\boldsymbol{v}_k), & a \neq b \end{cases}
\end{aligned} \tag{31}$$

Table 1 Nominal impulses described in the chaser's LVLH frame

Impulse	k=1	k=2	k=3	k=4
t_k (s)	13455.821	23889.631	58617.161	84168.071
Δv_{kx} (m/s)	−0.7007	−2.4560	0.6723	1.8463
Δv_{ky} (m/s)	12.6825	8.0886	−0.6618	16.2127
Δv_{kz} (m/s)	1.5309	4.2760	−1.0802	−3.3895

where $i, j = 1, 2, \cdots, 6; k = 1, 2, \cdots, m; \boldsymbol{\sigma}(\delta\Delta\boldsymbol{v}_k) = \alpha\,|\Delta\boldsymbol{v}_k| + \beta, \Delta\boldsymbol{v}_k$ is presented in Table 1, and $a, b = 1, 2, 3$. Obviously, the initial position and velocity uncertainties are correlated, and the three components of an impulse uncertainty are also correlated.

5.1 Accuracy comparison of the modified STTs

A problem of relative orbit propagation is first used to verify the accuracy of the derived STTs. An initial relative state in the chaser's LVLH frame, $\delta\boldsymbol{x}(t_0) = [-1.35$ km, -50 km, 0.1 km, 0.5 m/s, 2.323 m/s, 0.1 m/s$]^{\rm T}$, is propagated to the final time t_f using the STTs in Eq. (14). To obtain the exact solution, the relative state $\delta\boldsymbol{x}(t_0)$ is transformed to an absolute state $\tilde{\boldsymbol{x}}_{\rm cha}(t_0)$, then numerically integrating both the nominal state $\boldsymbol{x}_{\rm cha}(t_0)$ and the real $\tilde{\boldsymbol{x}}_{\rm cha}(t_0)$ to the final time using the dynamics of Eq. (1), and differencing them to obtain $\delta\boldsymbol{x}(t_f)$. The propagation errors compared to the exact solution $\delta\boldsymbol{x}(t_f)$ for different orders of STTs are presented in Table 2.

As shown in Table 2, for this problem with a large initial separation distance ($\approx$ 51 km), the 1st order STM has a big propagation error (around 121 km). In contrast, the 4th order STTs have only 2.826 km of position error after 1-day propagation. The higher order of the STTs, the better accuracy. These results indicate that the modified STTs can account for abrupt state jumps in the nominal trajectory.

5.2 Results of segmented uncertainty propagation

For the uncertainty propagation with impulsive maneuvers, the mean and covariance can be piecewise propagated to the final time using Eq. (B1) in Appendix B. The projected final position and velocity uncertainties are compared in Figs. 2–3 and Figs. 4–5, respectively. The MC simulations are assumed to provide the true distribution of the final uncertainty. For the segmented uncertainty propagation, the absolute computation errors of different solutions with respect to the MC

Table 2 Absolute errors of relative orbit propagation for different orders of STTs

Propagation error	1-order	2-order	3-order	4-order
Magnitude of relative position (m)	121684.99	3520.65	2925.48	2825.91
Magnitude of relative velocity (m/s)	139.707	4.079	3.392	3.269

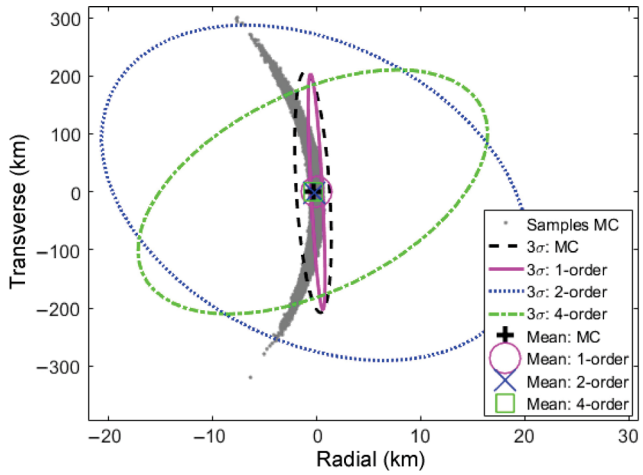

Fig. 2 Final position uncertainty in xy plane for segmented propagation.

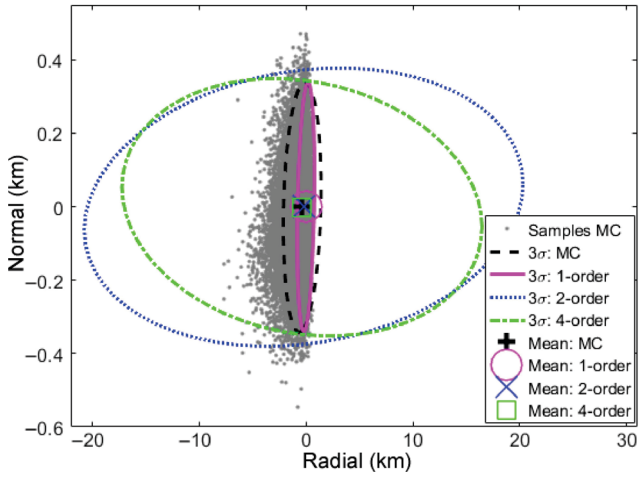

Fig. 3 Final position uncertainty in xz plane for segmented propagation.

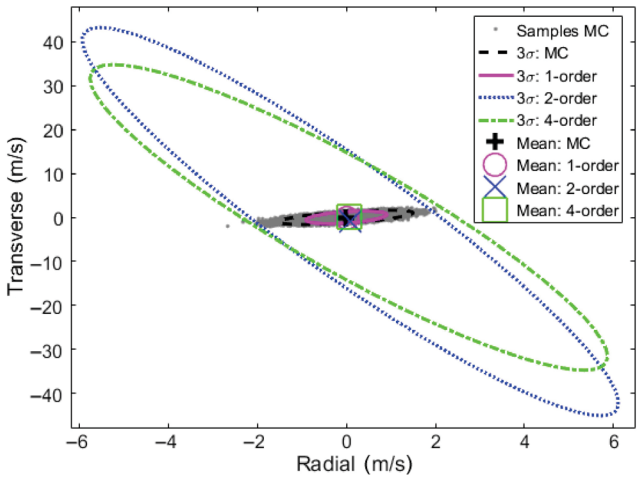

Fig. 4 Final velocity uncertainty in $v_x v_y$ plane for segmented propagation.

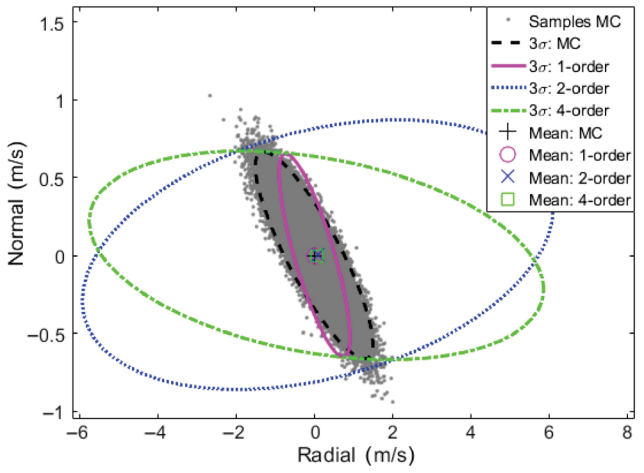

Fig. 5 Final velocity uncertainty in $v_x v_z$ plane for segmented propagation.

method are compared in Tables 3 and 4. For example, "(1-order)-MC" means that the result of 1-order solution minus the result of MC method.

As shown in Figs. 2–5, the position and velocity uncertainties propagated using the regular STTs have larger 3σ ellipsoids than those propagated using MC method. Evidently, most of the state spaces covered by the 3σ ellipsoids of the STTs include no MC samples, which means that the final uncertainty is almost impossible to occur in those areas. Therefore, the segmented uncertainty propagation using the regular STTs leads to inaccurate 3σ ellipsoids which are very different from the results of MC simulations. Moreover, the results of higher-order (2–4) STTs even become worse than the 1-order STM. If there are no abrupt state jumps, the enlarged 3σ ellipsoids of higher-order STTs should match well the MC results [9,10]. However, for the cases with abrupt state jumps, when the nonlinear terms ($\geqslant$ 2nd order) are included, the Taylor approximation error of Eq. (B1) will be recursively enlarged by the segmented STTs, as explained in Section 3.2. Therefore, the characteristics of nonlinear methods (2–4 orders of STTs) are different from the linear STM method. If only the nonlinear (2–4 orders) methods are compared, we can find that the higher order of the STTs, the better accuracy, because the higher-order STTs can reduce the approximation errors.

As shown in Tables 3 and 4, the results of higher-order ($\geqslant$ 2) STTs have large propagation errors with respect to the MC method, especially in transverse

Table 3 Final means in LVLH frame for segmented uncertainty propagation

Segmented STTs	m_x (m)	m_y (m)	m_z (m)	m_{vx} (mm/s)	m_{vy} (mm/s)	m_{vz} (mm/s)
MC	−356.63	−4.06	−1.20	−7.04	−1.36	0.64
(1-order)-MC	356.63	4.06	1.20	7.04	1.36	−0.64
(2-order)-MC	149.29	−1442.45	0.35	91.65	−936.12	4.39
(3-order)-MC	1246.12	−3963.18	3.87	382.50	−2485.21	10.60
(4-order)-MC	−17.29	39.23	−0.06	56.14	27.12	0.11

Table 4 Final standard deviations in LVLH frame for segmented uncertainty propagation

Segmented STTs	σ_x (m)	σ_y (m)	σ_z (m)	σ_{vx} (mm/s)	σ_{vy} (mm/s)	σ_{vz} (mm/s)
MC	588.74	69382.40	113.45	501.68	538.34	221.37
(1-order)-MC	−319.64	−1706.94	−0.30	−199.67	−65.80	−4.11
(2-order)-MC	6250.49	27008.55	12.94	1508.14	14185.11	67.30
(3-order)-MC	5176.97	3258.54	4.95	1578.04	11229.10	7.21
(4-order)-MC	5021.30	750.93	3.43	1437.35	11053.54	1.94

direction. For instance, the absolute errors of 2-order STTs are 1.44 and 27.0 km for the transverse mean m_y and transverse standard deviation σ_y, respectively. These absolute errors are larger than the 1st order STM. Therefore, the segmented uncertainty propagation with higher-order ($\geqslant 2$) STTs are not suitable for the problem with impulsive maneuvers.

5.3 Results of transitive uncertainty propagation

If the first-order assumption is adopted on the governing dynamics (i.e., $K = 1$ in Eq. (7)), the obtained STM is inherently transitive, i.e., $\boldsymbol{\Phi}^{i,l_1}_{(t_f,t_0)} = \boldsymbol{\Phi}^{i,k_1}_{(t_f,t_j)}\boldsymbol{\Phi}^{k_1,l_1}_{(t_j,t_0)}$. Thus, the first-order segmented propagation is the same with the first-order transitive propagation. However, the first-order method has low precision for a nonlinear dynamical system. In order to validate the accuracy of uncertainty propagation with the modified STTs in Eq. (13), we compare the STT-based methods with the MC method in Figs. 6–9 and Tables 5 and 6.

As shown in Figs. 6 and 7, the 3σ ellipsoids of the first-order method are smaller than the MC method, and thus less MC samples are included in its 3σ ellipsoids, especially in the radial direction. However, the modified STTs have almost the same 3σ ellipsoids with the MC method. In particular, the propagation error on radial position is sharply reduced in comparison to the first-order method.

As shown in Tables 5 and 6, for the 1-order method, the absolute errors of radial mean m_x and radial standard deviation σ_x are 356.63 and −319.64 m, respectively. However, these absolute errors for the

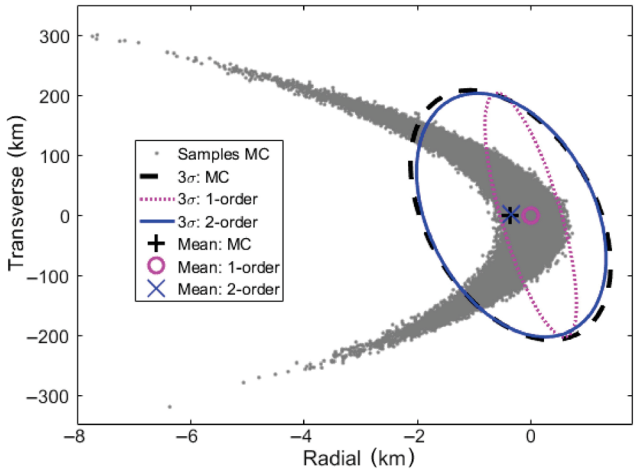

Fig. 6 Final position uncertainty in xy plane for transitive propagation.

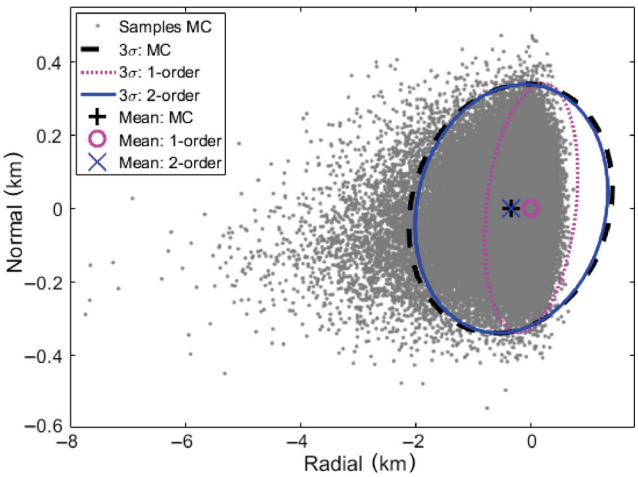

Fig. 7 Final position uncertainty in xz plane for transitive propagation.

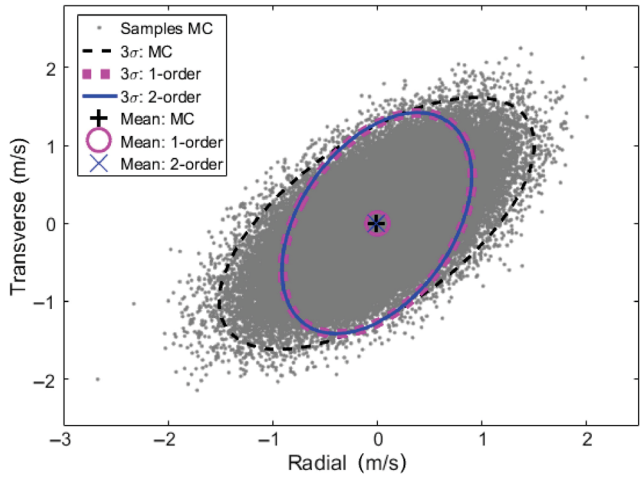

Fig. 8 Final velocity uncertainty in $v_x v_y$ plane for transitive propagation.

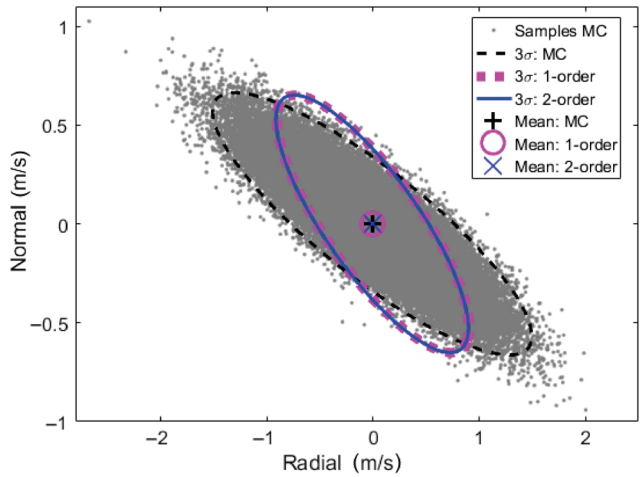

Fig. 9 Final velocity uncertainty in $v_x v_z$ plane for transitive propagation.

2-order modified STTs are only 14.37 and −31.16 m, respectively. Obviously, the radial propagation error is sharply reduced when taking the nonlinear terms into account. We can see that the transverse mean error of the modified STTs (11.53 m) is worse than the 1-order method (4.06 m). In fact, this deficiency is very small compared to the big transverse standard deviation (69.382 km). On the contrary, the improvements in radial mean (from 356.63 to 14.37 m) are countable after the nonlinear term is included. As illustrated in Figs. 6 and 7, the modified STT-based method outperforms the 1-order method and provides good agreement with the MC simulations.

In summary, comparing the results in Tables 3 and 4 with those in Tables 5 and 6, we can conclude that the transitive uncertainty propagation with the modified STTs in Eq. (13) is more accurate than the segmented uncertainty propagation in Eq. (B1) for problems with abrupt state jumps in the trajectory. Moreover, based on the results in Tables 2, 5, and 6, we find that higher-order STTs offer better accuracy with the tradeoff of requiring more computational efforts. As shown in Figs. 6 and 7, the second-order STTs can well match the MC results. Therefore, in order to reduce computational efforts, there is no need to use higher-order STTs in these test cases.

5.4 Results of GMM_STT method

As shown by the MC samples in Figs. 6 and 7, the initial Gaussian uncertainty becomes non-Gaussian after a nonlinear mapping of Eq. (1). Although the modified STT-based method provides good agreement with MC simulations on mean and covariance matrix propagation, the first two moments are insufficient to fully describing the non-Gaussian distribution. Therefore, the GMM_STT method presented in Section 4.2 is used to approximate the PDF of the final uncertainty.

The accuracy of the GMM method is quantified using

Table 5 Final means in LVLH frame for transitive uncertainty propagation

Transitive STTs	m_x (m)	m_y (m)	m_z (m)	m_{vx} (mm/s)	m_{vy} (mm/s)	m_{vz} (mm/s)
MC	−356.63	−4.06	−1.20	−7.04	−1.36	0.64
(1-order)-MC	356.63	4.06	1.20	7.04	1.36	−0.64
(2-order)-MC	14.37	11.53	0.05	0.35	4.16	−0.00
(GMM_STT)-MC	14.49	11.53	0.05	0.35	4.16	−0.00

Table 6 Final standard deviations in LVLH frame for transitive uncertainty propagation

Transitive STTs	σ_x (m)	σ_y (m)	σ_z (m)	σ_{vx} (mm/s)	σ_{vy} (mm/s)	σ_{vz}(mm/s)
MC	588.74	69382.40	113.45	501.68	538.34	221.37
(1-order)-MC	−319.64	−1706.94	−0.30	−199.67	−65.80	−4.11
(2-order)-MC	−31.16	−1706.93	−0.29	−199.50	−65.78	−4.10
(GMM_STT)-MC	−31.86	−1718.90	−0.29	−199.54	−65.80	−4.13

the log-likelihood (LL) of the MC samples, i.e.,

$$LL = \sum_{j=1}^{M} \log \left(\sum_{i=1}^{L} \boldsymbol{\omega}_i p_{\mathrm{g}}(\boldsymbol{x}_j; \boldsymbol{m}_i, \boldsymbol{P}_i) \right) \tag{32}$$

where M is the total number of MC runs, M=100,000 in this study, and x_j is the jth MC sample point. The log-likelihood (LL) of the GMM_STT method for different orders of STTs are compared in Fig. 10, in which higher LL indicates a closer fit.

As shown in Fig. 10, the nonlinear propagations with higher-order (2–4) STTs have better accuracy by consistently having higher LLs than the linear propagation with 1-order STM. Moreover, the transitive uncertainty propagation with 2-order modified STTs has better LL than the segmented uncertainty propagation with 4-order STTs. According to Eq. (A1), the number of elements of STTs increases exponentially with its order, e.g., for the 6-dimensional dynamical system, 258 ($=6^3+6^2+6$) elements are needed to integrate for the 2-order STTs, but 9330 ($=6^5+6^4+6^3+6^2+6$) elements are needed to integrate for the 4-order STTs. Therefore, more computation burden is required for higher-order STTs. As shown in Fig. 10, the transitive uncertainty propagation with 2-order STTs has the best accuracy. In addition, the LLs of the nonlinear propagations (2- and 4-order STTs) reach their stable values after the number of Gaussian mixtures is more than 25. It means that 25 Gaussian mixtures can well fit the final uncertainty if they are propagated using the higher-order STTs. In contrast, for the linear method, the MC samples are badly fitted even using 39 Gaussian mixtures.

As an example, the detailed results of the GMM_STT method with the 2-order modified STTs and 25 Gaussian mixtures are presented in Figs. 11–12 and Tables 5–6. Figure 11 gives the final 25 Gaussian mixtures propagated using the 2-order modified STTs of Eq. (24). As is shown, the MC samples are well surrounded by the 3σ ellipsoids of the 25 Gaussian mixtures, and it illustrates that the GMM_STT method is effective to capture the non-Gaussian uncertainty. The PDF computed using Eq. (27) is further presented in Fig. 12, and it can be seen that the approximated PDF has contours which well match of the curvature of the MC samples.

The means and standard deviations of the GMM_STT method are given in Tables 5 and 6, and it can be seen that the GMM_STT method has the similar results with the pure STT method on mean and covariance propagation. Specifically, the GMM_STT method is slightly worse than the modified STT method, e.g., the propagation errors on m_x, σ_x, and σ_y. This is the difference between covariance realism and uncertainty realism. Because the initial Gaussian mixtures are not a perfect representation of the original Gaussian distribution, which results in a small loss in covariance realism. However, it is clear to see that the Gaussian mixtures accurately capture the overall PDF, as shown in Figs. 11 and 12.

In addition, the efficiency of the GMM_STT method lies in three aspects: (1) the modified STTs in Eq. (13) only need to integrate once along the nominal trajectory for propagating all the Gaussian mixtures; (2) the splitting of a univariate Gaussian distribution can be obtained offline and applied to multivariate case, which

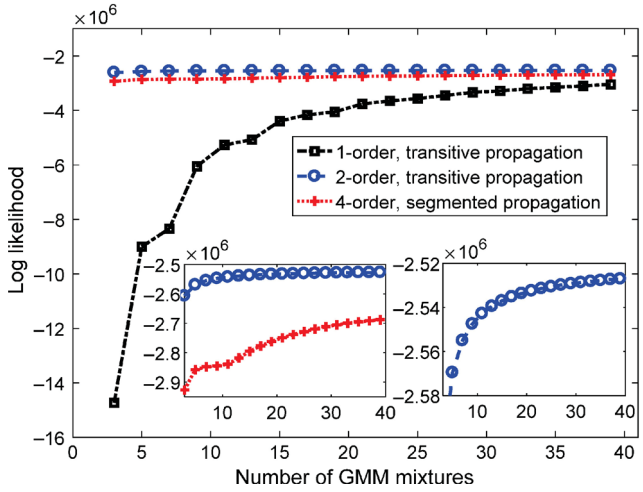

Fig. 10 Comparison of the log-likelihood for different orders of STTs.

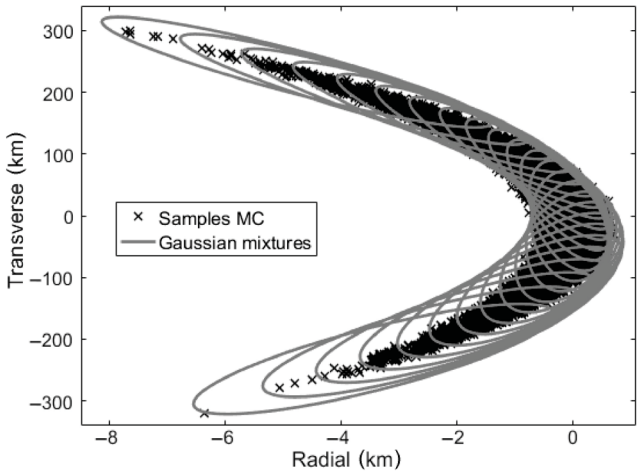

Fig. 11 Gaussian mixtures of GMM_STT method for final position uncertainty in xy plane.

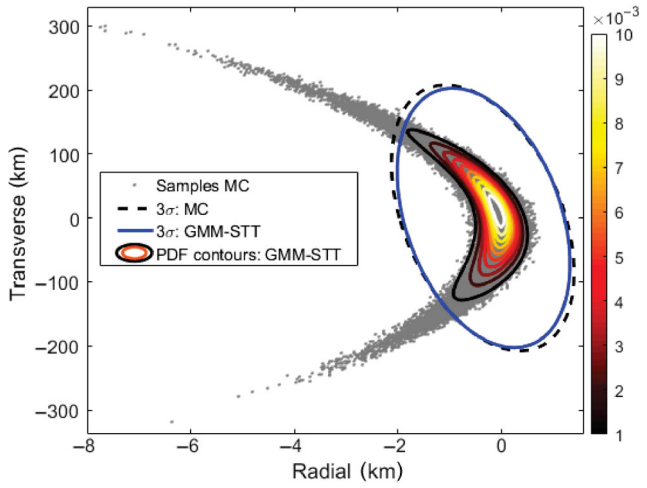

Fig. 12 PDF contours of GMM_STT method for final position uncertainty in xy plane.

can further reduce the computation burden; and (3) the GMM_STT method requires no random samples, which can avoid the curse of dimensionality for high-dimensional uncertainty propagation.

6 Conclusions

In order to propagate orbital uncertainty with impulsive maneuvers, a set of modified state transition tensors (STTs) is derived based on the regular STTs without maneuvers. The spacecraft's trajectory is divided into several segments by the impulsive maneuvers, and the modified STTs can connect these segmented trajectories together and allow for directly propagating uncertainty from the initial time to the final time. Analytical equations for propagating the mean and covariance matrix of navigation and maneuver uncertainties are obtained. The probability density function is also propagated using a method of combining the STTs and the Gaussian mixture model, in which the modified STTs are used to propagate the mean and covariance matrix of each Gaussian mixture. Because the modified STTs only need to integrate once along the nominal trajectory, and the splitting of input uncertainty can be performed using an offline univariate splitting library, the proposed uncertainty propagation method is quite efficient. Numerical results show that the proposed method provides good agreement with Monte Carlo simulations, and that the proposed method outperforms the previous STT-based method and the linear covariance propagation method.

Appendix A: Differential equation of STTs

The differential equations of STTs presented here are directly obtained from Ref. [9]. However, some symbols are changed in accordance with the expression in this study. The STTs up to the fourth order are expressed as follows:

$$
\begin{aligned}
\dot{\boldsymbol{\Phi}}^{i,\alpha} &= \boldsymbol{f}^{i,a}\boldsymbol{\Phi}^{a,\alpha}\\
\dot{\boldsymbol{\Phi}}^{i,\alpha\beta} &= \boldsymbol{f}^{i,a}\boldsymbol{\Phi}^{a,\alpha\beta} + \boldsymbol{f}^{i,ab}\boldsymbol{\Phi}^{a,\alpha}\boldsymbol{\Phi}^{b,\beta}\\
\dot{\boldsymbol{\Phi}}^{i,\alpha\beta\gamma} &= \boldsymbol{f}^{i,a}\boldsymbol{\Phi}^{a,\alpha\beta\gamma} + \boldsymbol{f}^{i,ab}\big(\boldsymbol{\Phi}^{a,\alpha}\boldsymbol{\Phi}^{b,\beta\gamma} + \boldsymbol{\Phi}^{a,\alpha\beta}\boldsymbol{\Phi}^{b,\gamma}\\
&\quad + \boldsymbol{\Phi}^{a,\alpha\gamma}\boldsymbol{\Phi}^{b,\beta}\big) + \boldsymbol{f}^{i,abc}\boldsymbol{\Phi}^{a,\alpha}\boldsymbol{\Phi}^{b,\beta}\boldsymbol{\Phi}^{c,\gamma}\\
\dot{\boldsymbol{\Phi}}^{i,\alpha\beta\gamma\theta} &= \boldsymbol{f}^{i,a}\boldsymbol{\Phi}^{a,\alpha\beta\gamma\theta} + \boldsymbol{f}^{i,ab}\big(\boldsymbol{\Phi}^{a,\alpha\beta\gamma}\boldsymbol{\Phi}^{b,\theta}\\
&\quad + \boldsymbol{\Phi}^{a,\alpha\beta\theta}\boldsymbol{\Phi}^{b,\gamma} + \boldsymbol{\Phi}^{a,\alpha\gamma\theta}\boldsymbol{\Phi}^{b,\beta} + \boldsymbol{\Phi}^{a,\alpha\beta}\boldsymbol{\Phi}^{b,\gamma\theta}\\
&\quad + \boldsymbol{\Phi}^{a,\alpha\gamma}\boldsymbol{\Phi}^{b,\beta\theta} + \boldsymbol{\Phi}^{a,\alpha\theta}\boldsymbol{\Phi}^{b,\beta\gamma} + \boldsymbol{\Phi}^{a,\alpha}\boldsymbol{\Phi}^{b,\beta\gamma\theta}\big)\\
&\quad + \boldsymbol{f}^{i,abc}\big(\boldsymbol{\Phi}^{a,\alpha\beta}\boldsymbol{\Phi}^{b,\gamma}\boldsymbol{\Phi}^{c,\theta} + \boldsymbol{\Phi}^{a,\alpha\gamma}\boldsymbol{\Phi}^{b,\beta}\boldsymbol{\Phi}^{d,\theta}\\
&\quad + \boldsymbol{\Phi}^{a,\alpha\theta}\boldsymbol{\Phi}^{b,\beta}\boldsymbol{\Phi}^{c,\gamma} + \boldsymbol{\Phi}^{a,\alpha}\boldsymbol{\Phi}^{b,\beta\gamma}\boldsymbol{\Phi}^{c,\theta}\\
&\quad + \boldsymbol{\Phi}^{a,\alpha}\boldsymbol{\Phi}^{b,\beta\theta}\boldsymbol{\Phi}^{c,\gamma} + \boldsymbol{\Phi}^{a,\alpha}\boldsymbol{\Phi}^{b,\beta}\boldsymbol{\Phi}^{c,\gamma\theta}\big)\\
&\quad + \boldsymbol{f}^{i,abcd}\boldsymbol{\Phi}^{a,\alpha}\boldsymbol{\Phi}^{b,\beta}\boldsymbol{\Phi}^{c,\gamma}\boldsymbol{\Phi}^{d,\theta}
\end{aligned}
\tag{A1}
$$

where $\boldsymbol{f}^{i,k_1\cdots k_p}(t) = \partial^p \boldsymbol{f}^i[t,x(t)]/\partial\boldsymbol{x}^{k_1}\cdots\partial\boldsymbol{x}^{k_p}$ is the higher-order partials of the dynamics along the reference trajectory, and $\boldsymbol{f}^{i,k_1\cdots k_p}$ can be automatically derived using the symbolic toolbox of MATLAB software. Based on Eq. (A1), $\boldsymbol{\Phi}^{i,l_1\cdots l_p}$ can be calculated using numerical integration, e.g., the Runge–Kutta method, and the initial conditions for these STTs are: $\boldsymbol{\Phi}_0^{i,\alpha} = 1$ if $i = \alpha$, and all the other initial STTs are zero.

Appendix B: Segmented uncertainty propagation using STTs

According to Ref. [12], the segmented propagation of mean and covariance matrix using the second-order ($K = 2$) STTs can be expressed as follows:

$$
\begin{cases}
\boldsymbol{m}^i(t_{k+1}) = \boldsymbol{\Phi}^{i,a}_{(t_{k+1},t_k)}(m_k^a)^+\\
\qquad\qquad + \dfrac{1}{2}\boldsymbol{\Phi}^{i,ab}_{(t_{k+1},t_k)}[(\boldsymbol{P}_k^{ab})^+ + (\boldsymbol{m}_k^a)^+(\boldsymbol{m}_k^b)^+]\\
\boldsymbol{P}^{ij}(t_{k+1}) = \boldsymbol{\Phi}^{i,a}_{(t_{k+1},t_k)}\boldsymbol{\Phi}^{j,b}_{(t_{k+1},t_k)}[(\boldsymbol{P}_k^{ab})^+\\
\qquad\qquad + (\boldsymbol{m}_k^a)^+(\boldsymbol{m}_k^b)^+] + \dfrac{1}{2}(\boldsymbol{\Phi}^{i,a}_{(t_{k+1},t_k)}\boldsymbol{\Phi}^{j,bc}_{(t_{k+1},t_k)}\\
\qquad\qquad + \boldsymbol{\Phi}^{j,a}_{(t_{k+1},t_k)}\boldsymbol{\Phi}^{i,bc}_{(t_{k+1},t_k)})(E[\delta\boldsymbol{x}_k^a\delta\boldsymbol{x}_k^b\delta\boldsymbol{x}_k^c])^+\\
\qquad\qquad + \dfrac{1}{4}\boldsymbol{\Phi}^{i,ab}_{(t_{k+1},t_k)}\boldsymbol{\Phi}^{j,cd}_{(t_{k+1},t_k)}(E[\delta\boldsymbol{x}_k^a\delta\boldsymbol{x}_k^b\delta\boldsymbol{x}_k^c\delta\boldsymbol{x}_k^d])^+\\
\qquad\qquad - \boldsymbol{m}_{k+1}^i\boldsymbol{m}_{k+1}^j
\end{cases}
\tag{B1}
$$

where $\boldsymbol{\Phi}_{(t_{k+1},t_k)}$ is the STTs from the kth maneuver time t_k to the $(k+1)$th maneuver time t_{k+1}, and the superscript "+" indicates the state after an impulse; $k = 0, 1, \cdots, m, t_{m+1} = t_f$, $\boldsymbol{m}_0^+ = \boldsymbol{m}_0$, $\boldsymbol{m}_k^+ = \boldsymbol{m}_k + \boldsymbol{m}_{kv}$, $\boldsymbol{P}_0^+ = \boldsymbol{P}_0$, and $\boldsymbol{P}_k^+ = \boldsymbol{P}_k + \boldsymbol{P}_{kv}, \boldsymbol{m}_{kv}$ and $\boldsymbol{P}_{kv}$ are the same with those in Eq. (22). Let $\boldsymbol{m}_0 = \boldsymbol{m}_k^+$ and $\boldsymbol{P}_0 = \boldsymbol{P}_k^+$, then the third and fourth moments at post maneuver times, i.e., $(E[\delta\boldsymbol{x}_k^a\delta\boldsymbol{x}_k^b\delta\boldsymbol{x}_k^c])^+$ and $(E[\delta\boldsymbol{x}_k^a\delta\boldsymbol{x}_k^b\delta\boldsymbol{x}_k^c\delta\boldsymbol{x}_k^d])^+$, can be computed using Eq. (17). It is noted that the segmented propagation of mean and covariance matrix using higher-order STTs (e.g., $K = 3, 4$) is similar with Eq. (B1).

Acknowledgements

The authors acknowledge the financial support from the National Natural Science Foundation of China (Nos. 11222215 and 11572345), the National Basic Research Program of China (973 Program, No. 2013CB733100), and the Program for New Century Excellent Talents in University (No. NCET-13-0159).

References

[1] Rovetto, R. J., Kelso, T. S. Preliminaries of a space situational awareness ontology. In: Proceedings of the 26th AIAA/AAS Space Flight Mechanics Meeting, **2016**.

[2] Battin, R. H. *An Introduction to the Mathematics and Methods of Astrodynamics*. American Institute of Aeronautics and Astronautics, **1999**.

[3] Geller, D. K. Linear covariance techniques for orbital rendezvous analysis and autonomous onboard mission planning. *Journal of Guidance, Control, and Dynamics*, **2006**, 29(6): 1404–1414.

[4] Sabol, C., Hill, K., Alfriend, K., Sukut, T. Nonlinear effects in the correlation of tracks and covariance propagation. *Acta Astronautica*, **2013**, 84: 69–80.

[5] Vittaldev, V., Russell, R. P. Space object collision probability via Monte Carlo on the graphics processing unit. *The Journal of the Astronautical Sciences*, **2017**, 64(3): 285–309.

[6] Junkins, J. L., Akella, M. R., Alfriend, K. T. Non-Gaussian error propagation in orbital mechanics. *Guidance and Control*, **1996**, 1996: 283–298.

[7] Junkins, J. L., Singla, P. How nonlinear is it? A tutorial on nonlinearity of orbit and attitude dynamics. *Advances in the Astronautical Sciences*, **2003**, 115(SUPPL.): 1–45.

[8] Julier, S. J., Uhlmann, J. K. Unscented filtering and nonlinear estimation. *Proceedings of the IEEE*, **2004**, 92(3): 401–422.

[9] Park, R. S., Scheeres, D. J. Nonlinear mapping of Gaussian statistics: Theory and applications to spacecraft trajectory design. *Journal of Guidance, Control, and Dynamics*, **2006**, 29(6): 1367–1375.

[10] Fujimoto, K., Scheeres, D. J., Alfriend, K. T. Analytical nonlinear propagation of uncertainty in the two-body problem. *Journal of Guidance, Control, and Dynamics*, **2012**, 35(2): 497–509.

[11] Park, I., Scheeres, D. J. Hybrid method for uncertainty propagation of orbital motion. *Journal of Guidance, Control, and Dynamics*, **2018**, 41(1): 240–254.

[12] Yang, Z., Luo, Y.-Z., Zhang, J., Tang, G.-J. Uncertainty quantification for short rendezvous missions using a nonlinear covariance propagation method. *Journal of Guidance, Control, and Dynamics*, **2016**, 39(9): 2170–2178.

[13] Hernando-Ayuso, J., Bombardelli, C. Orbit covariance propagation via quadratic-order state transition matrix in curvilinear coordinates. *Celestial Mechanics and Dynamical Astronomy*, **2017**, 129(1–2): 215–234.

[14] Yang, Z., Luo, Y.-Z., Lappas, V., Tsourdos, A. Nonlinear analytical uncertainty propagation for relative motion near J_2-perturbed elliptic orbits. *Journal of Guidance, Control, and Dynamics*, **2018**, 41(4): 888–903.

[15] Berz, M. *Modern Map Methods in Particle Beam Physics*. Academic Press, **1999**.

[16] Valli, M., Armellin, R., Di Lizia, P., Lavagna, M. R. Nonlinear mapping of uncertainties in celestial mechanics. *Journal of Guidance, Control, and Dynamics*, **2013**, 36(1): 48–63.

[17] Morselli, A., Armellin, R., Di Lizia, P., Bernelli Zazzera, F. A high order method for orbital conjunctions analysis: Monte Carlo collision probability computation. *Advances in Space Research*, **2015**, 55(1): 311–333.

[18] Wittig, A., Di Lizia, P., Armellin, R., Makino, K., Bernelli-Zazzera, F., Berz, M. Propagation of large uncertainty sets in orbital dynamics by automatic domain splitting. *Celestial Mechanics and Dynamical Astronomy*, **2015**, 122(3): 239–261.

[19] Wittig, A., Colombo, C., Armellin, R. Long-term density evolution through semi-analytical and differential algebra techniques. *Celestial Mechanics and Dynamical Astronomy*, **2017**, 128(4): 435–452.

[20] Riccardi, A., Tardioli, C., Vasile, M. An intrusive approach to uncertainty propagation in orbital mechanics based on Tchebycheff polynomial algebra. In: *Astrodynamics 2015. Advances in Astrnautical Sciences*. American Astronautical Society, **2015**: 707–722.

[21] Jones, B. A., Doostan, A., Born, G. H. Nonlinear propagation of orbit uncertainty using non-intrusive polynomial chaos. *Journal of Guidance, Control, and Dynamics*, **2013**, 36(2): 430–444.

[22] Jones, B. A., Doostan, A. Satellite collision probability estimation using polynomial chaos expansions. *Advances in Space Research*, **2013**, 52(11): 1860–1875.

[23] Jones, B. A., Parrish, N., Doostan, A. Postmaneuver collision probability estimation using sparse polynomial chaos expansions. *Journal of Guidance, Control, and Dynamics*, **2015**, 38(8): 1425–1437.

[24] Vetrisano, M., Vasile, M. Analysis of spacecraft disposal solutions from LPO to the Moon with high order polynomial expansions. *Advances in Space Research*, **2017**, 60(1): 38–56.

[25] Bierbaum, M. M., Joseph, R. I., Fry, R. L., Nelson, J. B. A Fokker–Planck model for a two-body problem. *AIP Conference Proceedings*, **2002**, 617(1): 340–371.

[26] Horwood, J. T., Aragon, N. D., Poore, A. B. Gaussian sum filters for space surveillance: Theory and simulations. *Journal of Guidance, Control, and Dynamics*, **2011**, 34(6): 1839–1851.

[27] DeMars, K. J., Bishop, R. H., Jah, M. K. Entropy-based approach for uncertainty propagation of nonlinear dynamical systems. *Journal of Guidance, Control, and Dynamics*, **2013**, 36(4): 1047–1057.

[28] Vishwajeet, K., Singla, P., Jah, M. Nonlinear uncertainty propagation for perturbed two-body orbits. *Journal of Guidance, Control, and Dynamics*, **2014**, 37(5): 1415–1425.

[29] Vittaldev, V., Russell, R. P. Space object collision probability using multidirectional Gaussian mixture models. *Journal of Guidance, Control, and Dynamics*, **2016**, 39(9): 2163–2169.

[30] Fujimoto, K., Scheeres, D. J. Tractable expressions for nonlinearly propagated uncertainties. *Journal of Guidance, Control, and Dynamics*, **2015**, 38(6): 1146–1151.

[31] Vittaldev, V., Russell, R. P., Linares, R. Spacecraft uncertainty propagation using Gaussian mixture models and polynomial chaos expansions. *Journal of Guidance, Control, and Dynamics*, **2016**, 39(12): 2615–2626.

[32] Luo, Y.-Z., Yang, Z. A review of uncertainty propagation in orbital mechanics. *Progress in Aerospace Sciences*, **2017**, 89: 23–39.

[33] Vallado, D. A. *Fundamentals of Astrodynamics and Applications, 3rd edn.* Microscosm Press, **2007**.

[34] Fehse, W. *Automated Rendezvous and Docking of Spacecraft*. Cambridge University Press, **2003**.

[35] Phillips, K. R function to symbolically compute the central moments of the multivariate normal distribution. *Journal of Statistical Software*, **2010**, 33(1): 1–14.

[36] Terejanu, G., Singla, P., Singh, T., Scott, P. D. Uncertainty propagation for nonlinear dynamic systems using Gaussian mixture models. *Journal of Guidance, Control, and Dynamics*, **2008**, 31(6): 1623–1633.

[37] Yang, Z., Luo, Y.-Z., Zhang, J., Tang, G.-J. Homotopic perturbed Lambert algorithm for long-duration rendezvous optimization. *Journal of Guidance, Control, and Dynamics*, **2015**, 38(11): 2215–2223.

Zhen Yang received his B.S., M.S., and Ph.D. degrees in aerospace engineering from National University of Defense Technology, China, in 2011, 2013, and 2018, respectively. He was a visiting scholar of Cranfield University, UK, in 2016. After graduation from doctoral, he joined National University of Defense Technology as a lecturer in 2018. His current research interests include astrodynamics, uncertainty quantification, and space trajectory optimization. E-mail: yangzhen@nudt.edu.cn.

Ya-Zhong Luo received his B.S., M.S., and Ph.D. degrees in aerospace engineering from National University of Defense Technology, China, in 2001, 2003, and 2007, respectively. Since December 2013, he has been a professor in National University of Defense Technology. His current research interests include manned spaceflight mission planning, spacecraft dynamics and control, and evolutionary computation. E-mail: luoyz@nudt.edu.cn.